# Project 064 Alternative Design Configurations to Meet Future Demand

## Georgia Institute of Technology

## Project Lead Investigator

Prof. Dimitri N. Mavris
Director, Aerospace Systems Design Laboratory
School of Aerospace Engineering
Georgia Institute of Technology
Atlanta, GA 30332-0150
404-894-1557
dimitri.mavris@ae.gatech.edu

Dr. Michelle Kirby
Chief, Civil Aviation Division
Aerospace Systems Design Laboratory
School of Aerospace Engineering
Georgia Institute of Technology
Atlanta, GA 30332-0150
404-385-2780
michelle.kirby@ae.gatech.edu

## University Participants

**Georgia Institute of Technology (Georgia Tech)**

- P.I.s: Dr. Dimitri N. Mavris and Dr. Michelle Kirby
- FAA Award Number: 13-C-AJFE-GIT-062
- Period of Performance: September 30, 2023, to September 30, 2024
- Tasks:
    1. Improvement of Advanced Concept Aircraft (ACA) representation in Modeling and Databases Group (MDG)/Forecasting and Economic Analysis Support Group (FESG) models
    2. Alternative design approaches to meet demand.
    3. Exploring physics-based boundaries of the possible

## Project Funding Level

The Federal Aviation Administration (FAA) provided $500,000 in funding, and Georgia Tech has agreed to a total of $500,000 in matching funds. This total includes salaries for the project director, research engineers, and graduate research assistants, as well as funds for computing, financial, and administrative support, including meeting arrangements. The Georgia Tech has also agreed to provide tuition remission for the students, paid from state funds.

## Investigation Team

Prof. Dimitri N. Mavris, (P.I.), All Tasks
Dr. Michelle Kirby, (co-P.I.), All Tasks
Dr. Jon Gladin, (technical lead), All Tasks
Dr. Yu Cai, (technical lead), All Tasks
Dr. Jiacheng Xie, (technical lead), All Tasks
Mr. Yaw Tung Tan, (graduate student researcher), Task 1
Ms. Nina Kondur, (graduate student researcher), Task 1
Mr. Felipe Zurita, (graduate student researcher), Task 1

Mr. Tuna Ergan, (graduate student researcher), Task 2
Ms. Yutong Cheng, (graduate student researcher), Task 2
Mr. Nicholas Cocoves, (graduate student researcher), Task 2
Mr. Ty Mancao, (graduate student researcher), Task 2
Ms. Salma Benhissoune, (graduate student researcher), Task 2
Ms. Akshiti Parashar, (graduate student researcher), Tasks 2 and 3
Mr. Cem Kocer, (graduate student researcher), Task 3
Ms. Emmanuella Okonkwo, (graduate student researcher), Task 3

# Project Overview

The purpose of ASCENT Project 064 is to improve upon the modeling approach used in the first two years of research and to provide insights or recommendations to the MDG regarding a more realistic approach to modeling ACA at the fleet level. In addition, the project will address alternative means of designing aircraft beyond the usual adoption of technologies with the payload and range capability of the existing fleet.

# Task 1 - Improvement of ACA Representation in MDG/FESG Models

**Georgia Institute of Technology**

## Objective

The objective of this task is to investigate potential opportunities for improving how ACAs are modeled within the fleet to benefit current analyses and probable future analyses. The traditional approach to modeling future aircraft types in the fleet has been to define a proxy aircraft that the new aircraft entering the fleet will replace and then establish a change in benefit. Although this process worked for evolutionary aircraft of the past, it does not work for ACAs, which may have markedly different performance behavior from that of conventional aircraft, such as different cruise altitudes and speeds or different range capabilities for the same seat class. To model an ACA within the MDG modeling tools, manufacturers would need to provide the necessary performance, emissions, and noise coefficients defined by Society of Automotive Engineers (SAE) Aerospace Information Report (AIR) 1845 and the Base Aircraft Data (BADA 3). Prior research in this area, specifically for a blended wing body (BWB), has shown limitations in the accuracy of these tools in capturing the expected performance.

Within the Environmental Design Space (EDS), algorithms exist to create the necessary performance, emissions, and noise coefficients needed by MDG's modeling tools. Although the coefficients can be determined, how the ACA actually flies within MDG tools may not be correct, and modifications to the framework may be required.

Building on these findings, the current objective is to enable ACA modelling and fleet assessment capability within the Aviation Environmental Design Tool (AEDT). Specifically, this year's work aims to establish and validate a data pipeline between EDS and AEDT to facilitate the transfer of ACA performance data. Once validated, the pipeline will be demonstrated by processing a BWB model developed in EDS, thus enabling ACA modeling capacity in AEDT.

## Research Approach

This year's research focused on a deep-dive validation of the EDS-to-AEDT data pipeline, correcting engine modeling discrepancies, and beginning the integration of ACA models.

**Step 1 – Tooling Development and Initial Discrepancy Investigation**

To make future analyses more efficient, internal tools were developed to enable comparative assessments of ACA and conventional tube-and-wing aircraft models simulated in the EDS and AEDT. An Airbus® A320neo was selected as the Technology Reference Aircraft (TRA) to serve as a control case for validating connectivity and consistency between the EDS and AEDT. The TRA model was developed in EDS and calibrated using public domain data for the Airbus A320neo and Pratt & Whitney® PW1100G engine.

® Airbus is a registered trademark of Airbus Operations GmbH, Hamburg, Germany.
® Pratt & Whitney is a registered trademark of RTX Corporation, Farmington, Connecticut.

When comparing the TRA departure trajectories between EDS and AEDT, a discrepancy was observed in the climb gradient above 4000 ft above field elevation (AFE), as depicted in Figure 1, despite both tools applying the same cutback thrust setting. Initial investigations focused on identifying the source of this difference between EDS and AEDT takeoff performance models, with checks on aerodynamic drag performance, takeoff procedure implementation and weight.

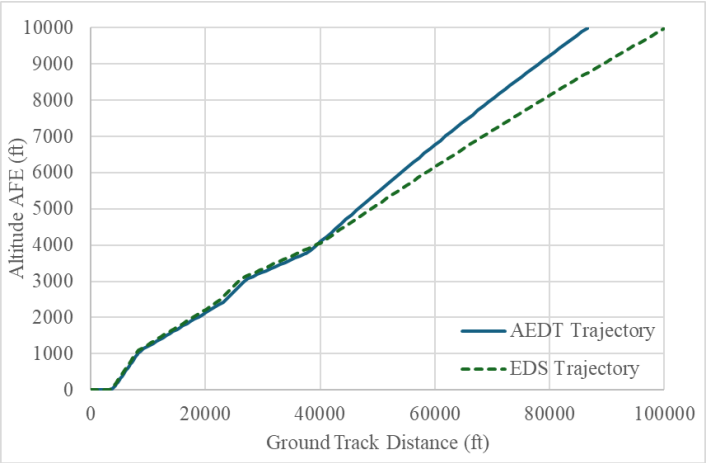


**Figure 1.** Trajectory discrepancy between Environmental Design Space (EDS) and Aviation Environmental Design Tool (AEDT). AFE: above field elevation.

**Step 2 – Engine Model Refinement and Calibration**

The root cause of the trajectory discrepancy was traced to a fundamental difference in thrust modeling between the two modeling environments:

- The EDS relies on a single lookup table (i.e., engine deck) of flight conditions, thrust, and fuel flow for all phases of flight. This model included a sharp transition from Maximum Takeoff (TO) thrust to Maximum Continuous (MCT) thrust at Mach 0.4, causing a sharp non-linear drop in thrust as depicted in Figure 2.
- The AEDT relies on different polynomials and models for different throttle settings. However, the sudden drop in maximum thrust due to the rating change is difficult for AEDT's polynomial-based thrust model to accurately capture, no matter how the coefficients are fitted, as seen in Figure 3. This created a significant thrust difference between the two models, ultimately causing the observed trajectory discrepancy.

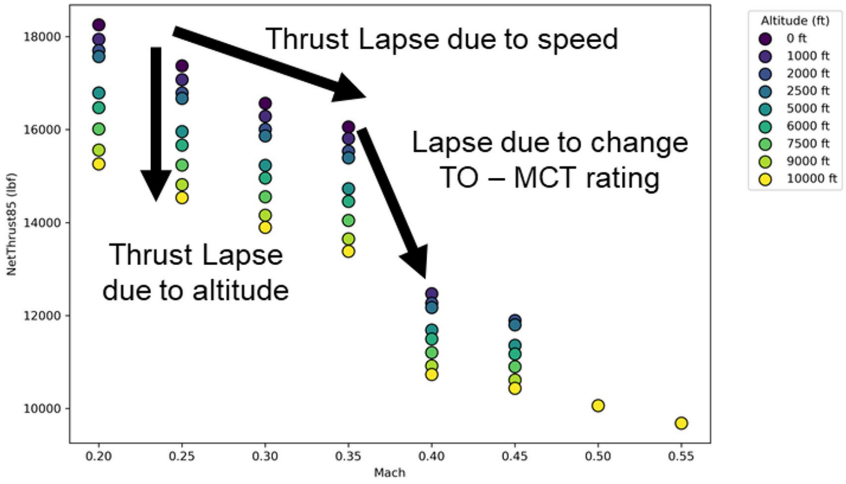


**Figure 2.** Non-linear drop in thrust due to the maximum thrust setting transition.

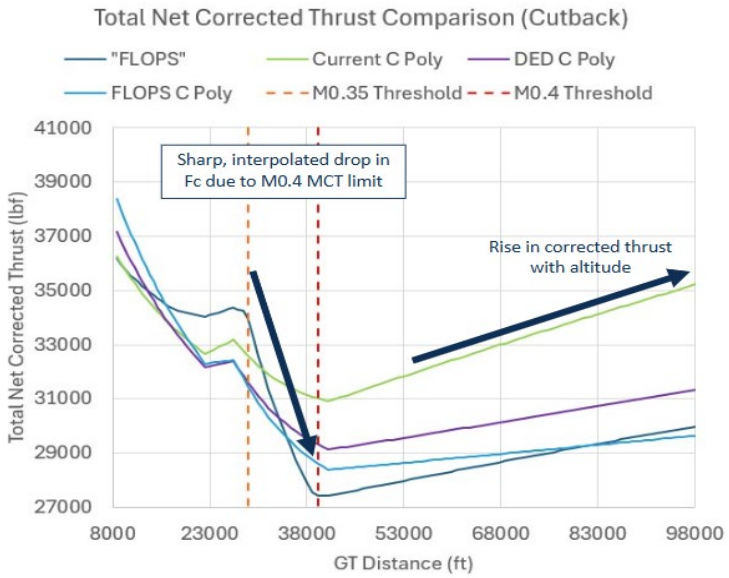


**Figure 3.** Difficulty in AEDT's polynomial-based model to capture thrust drop due to rating change at Mach (M) 0.4. FLOPS: Flight Optimization System.

A significant effort was made to resolve these thrust discrepancies between the models. This involved identifying and applying the corrections necessary to the climb power and rating modeling within EDS to produce a better fit using AEDT's aircraft nuclear propulsion jet thrust polynomial structure. Engine rating discrepancies were corrected in EDS by increasing the TO-MCT transition Mach number from 0.4 to 0.5 in EDS. This resolved thrust differences between the EDS engine deck and AEDT thrust polynomial models, enabling an improved polynomial fit. Figure 4 shows the improved thrust behavior after the fix. The main drawback of this method is that it may not fully represent real engine operating conditions, because the use of maximum takeoff thrust is typically limited to only a few minutes before transitioning to the MCT rating. However, because the departure procedure in this case applies an 85% thrust cutback rather than full power, this deviation from real operation is not expected to have a large impact on the overall results.

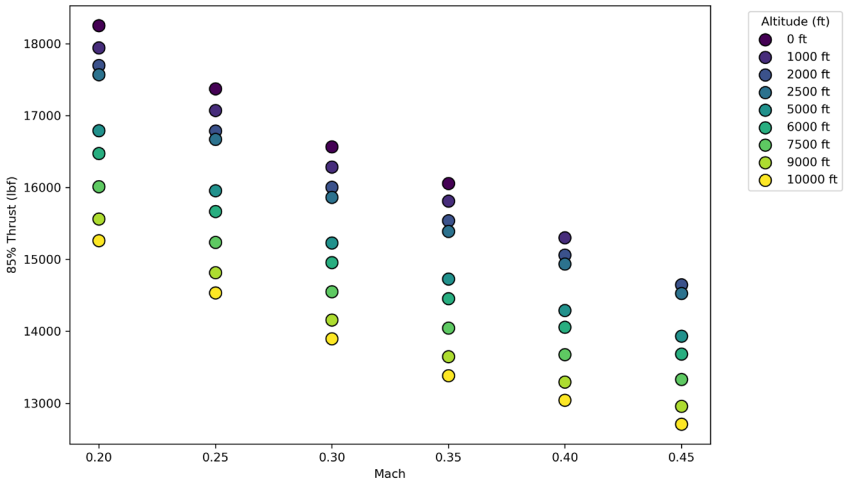


**Figure 4.** Thrust lapse after rating change set at Mach 0.5.

As part of this, the PW1133G-JM engine was re-calibrated in EDS to fix a thrust lapse issue, and a de-rated PW1129G-JM variant was developed for comparison with AEDT's A320neo BADA model. A new set of engine deck data was then generated using this modified rating structure for subsequent analysis.

**Step 3: Trajectory Analysis**

Following the thrust modeling refinement, the A320-271N model was simulated in both EDS and AEDT for the takeoff and landing phases to compare and check for consistent results. A set of 18 trajectories for the model was generated covering six stage lengths and three takeoff procedures. Figure 5 presents the takeoff comparison, showing altitude and net thrust versus ground track distance using a standard takeoff procedure and a mission range corresponding to stage length 1 (i.e.,350 nmi). The altitude profiles show a similar initial climb-out trajectory, but around 2,000 ft, the AEDT begins to overestimate thrust, causing an early constant speed climb. This creates a discrepancy in the final ground track distance, with the EDS model reaching 10,000 ft altitude at a ground distance of 4,144 ft after AEDT does. This deviation is primarily due to differences in physics modules and assumptions across the tools. The net thrust profiles show a much closer correlation, with a maximum deviation of only 9.5%. The takeoff trajectories are found to diverge beyond roughly 36,500 ft of ground track distance. As the trajectory deviation past 35,000 ft ground track distance has no effect on certification noise, this difference is considered to have a negligible effect on noise results. The final quantified weight and trajectory deviations across all 18 takeoff profiles are shown in Table 1 below.

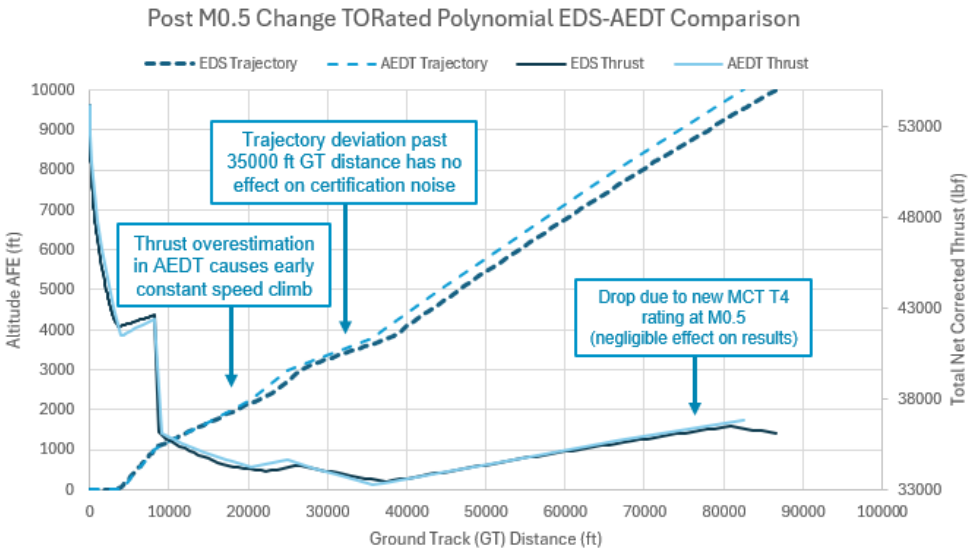


**Figure 5.** Takeoff trajectory comparison after thrust rating change. AEDT: Aviation Environmental Design Tool, AFE: above field elevation, EDS: Environmental Design Space, M: Mach.

**Table 1.** Departure trajectories comparison between EDS and AEDT. ICAO: International Civil Aviation Organization.

| Stage length | Profile | Max altitude deviation (ft) | Initial weight difference (lb) | End-point weight difference (lb) | Final distance error (nmi) |
|---|---|---|---|---|---|
| 1 | STANDARD | 463 | 1 | 2 | 0.682 |
| 1 | ICAO A | 501 | 1 | 9 | 0.742 |
| 1 | ICAO B | 469 | 1 | 6 | 0.691 |
| 2 | STANDARD | 458 | 2 | 4 | 0.706 |
| 2 | ICAO A | 489 | 2 | 10 | 0.761 |
| 2 | ICAO B | 448 | 2 | 5 | 0.682 |
| 3 | STANDARD | 456 | 2 | 5 | 0.725 |
| 3 | ICAO A | 484 | 2 | 13 | 0.785 |
| 3 | ICAO B | 426 | 2 | 6 | 0.684 |
| 4 | STANDARD | 520 | 2 | 17 | 0.898 |
| 4 | ICAO A | 503 | 2 | 15 | 0.874 |
| 4 | ICAO B | 408 | 2 | 8 | 0.73 |
| 5 | STANDARD | 564 | 2 | 29 | 1.068 |
| 5 | ICAO A | 526 | 2 | 26 | 1.014 |
| 5 | ICAO B | 401 | 2 | 10 | 0.767 |
| 6 | STANDARD | 567 | 3 | 32 | 1.093 |
| 6 | ICAO A | 540 | 3 | 35 | 1.053 |
| 6 | ICAO B | 404 | 3 | 11 | 0.793 |

An initial comparison of approach trajectories for Stage Length 1 was also completed. The landing comparison, shown in Figure 6, shows nearly identical trajectory plots for EDS and AEDT, but the thrust profiles show deviation. The AEDT assumes a specific reverse-thrust and braking procedure not modeled in EDS, leading to the large spike seen in the plot upon touchdown. Overall, this validation exercise demonstrates that the aerodynamic and propulsion characteristics of the EDS model are represented successfully within the AEDT.

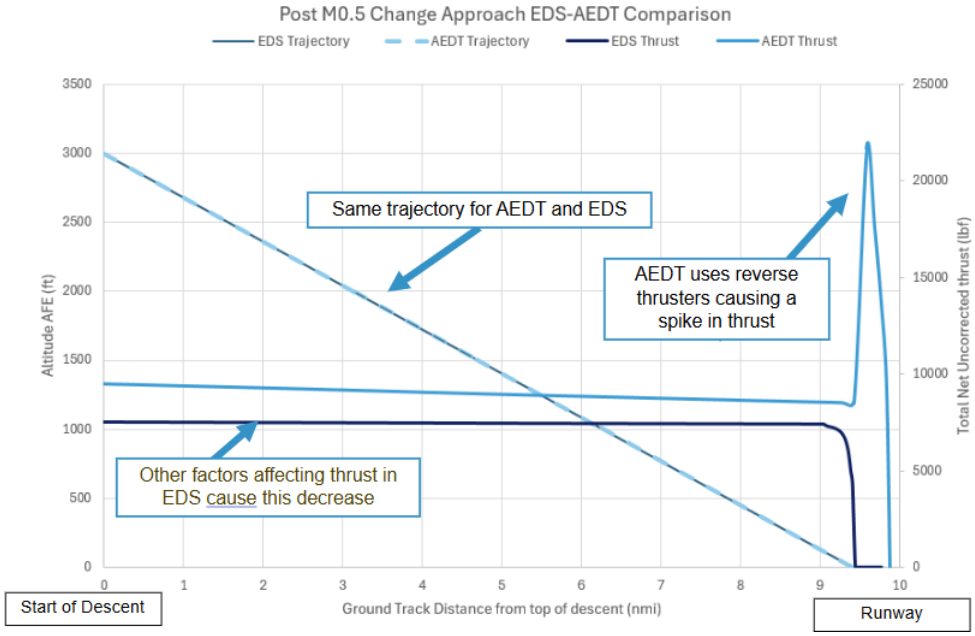


**Figure 6.** Approach trajectory comparison after thrust rating change. AEDT: Aviation Environmental Design Tool, AFE: above field elevation, EDS: Environmental Design Space, M: Mach.

**Step 4: ACA Model Development**

With the EDS-to-AEDT pipeline successfully validated, work commenced on modeling the target ACA. The ACA concept selected is a notional Blended Wing-Body (BWB) model, which was developed within the EDS framework by prior work in the lab. The model draws inspiration from JetZero®'s recent BWB concept. A three-view geometric layout of the ACA model generated in OpenVSP[1] is shown in Figure 7 below.

® JetZero is a registered trademark of Blended Wing Aircraft, Inc., Orange, California.

[1] OpenVSP is a parametric aircraft geometry tool. OpenVSP allows the user to create a 3D model of an aircraft defined by common engineering parameters. This model can be processed into formats suitable for engineering analysis. The predecessors to OpenVSP have been developed by J.R. Gloudemans and others for NASA since the early 1990's. On January 10, 2012. OpenVSP was released as an open-source project under the NASA Open-Source Agreement (NOSA) version 1.3.

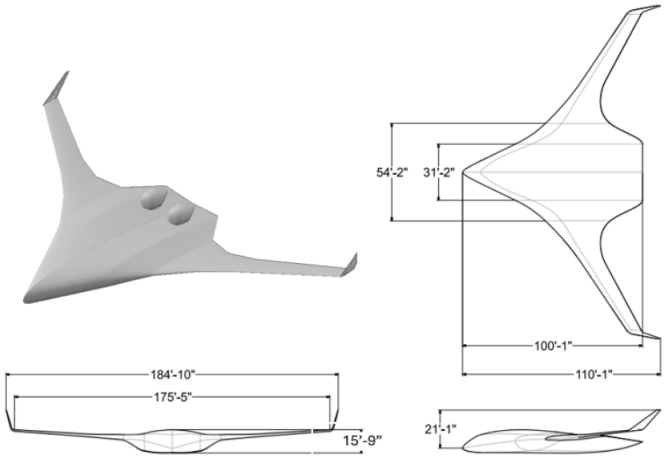


**Figure 7.** BWB model three-view layout.

The baseline geometry was aerodynamically optimized using a gradient-free approach along with high-fidelity computational fluid dynamics (CFD) analyses. The engine model used was derived from the current PW1133G geared turbofan and modified with an updated core and fan design to achieve a higher sea-level-static (SLS) thrust rating of approximately 43,000 lb. The notional engine model was developed using NPSS (Numerical Propulsion System Simulation) for cycle analysis and WATE++ for engine weights, based on the multi-point-design process. This 2030 variant features a larger fan, higher bypass and overall pressure ratios, and an improved lower thrust lapse rate, leading to lower specific fuel consumption and weight when compared to the baseline PW1133.

Some modifications were made to tailor the BWB model for the EDS-AEDT analysis. Specifically, the high-lift device deflections were revised to 12° for take-off flaps and 25° for landing flaps, and the aerodynamic performance inputs were adjusted with updated flap-induced drag increments to better capture the departure and approach segments effects rather than high-altitude and high-speed behaviors. A mission-level performance analysis was then conducted using the Flight Optimization System (FLOPS) tool, integrating the CFD-derived aerodynamic data and advanced propulsion model with an updated mission profile required for this analysis, as shown in Figure 8. The resulting key performance specifications for this mission are defined in Table 2.

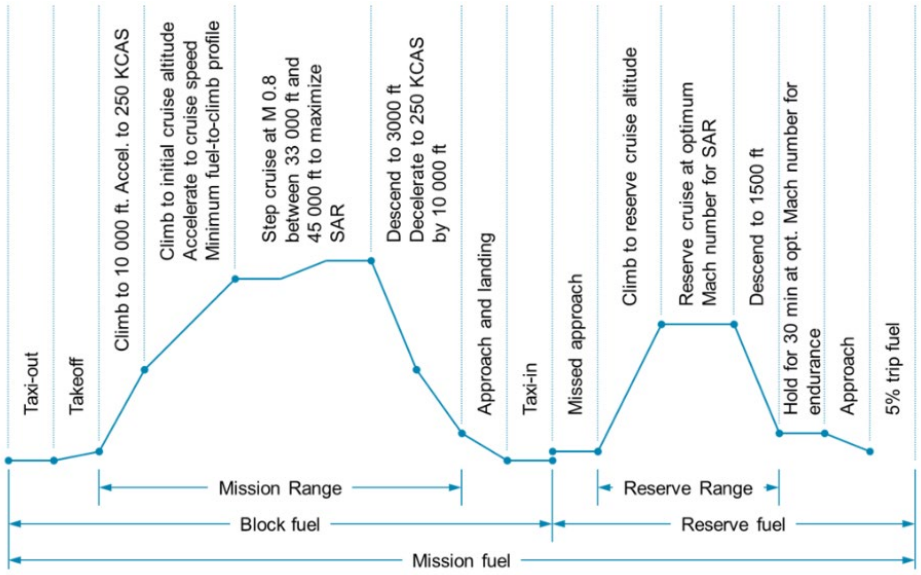


**Figure 8.** Mission profile of the ACA model. KCAS: Knots Calibrated Airspeed, M: Mach, SAR: specific air range.

**Table 2.** Key specifications of the ACA model with 2030 technologies infused PW1133G engine.

| Parameter | Value | Unit |
|---|---|---|
| **Design range** | 5000 | nmi |
| **Operational empty weight** | 143155 | lb |
| **Max takeoff weight** | 269987 | lb |
| **Max landing weight** | 209073 | lb |
| **Ramp weight** | 270415 | lb |
| **Design payload weight** | 56250 | lb |
| **Design fuel load** | 71010 | lb |
| **Thrust per engine** | 43000 | lb |
| **Wing loading** | 47.24 | $lbf/ft^2$ |
| **Thrust to weight ratio** | 0.318 | |

## Milestones

- Completed Step 1- Developed comparative analysis tooling and identified initial discrepancies.
- Completed Step 2 - Corrected engine rating and thrust modeling discrepancies, re-calibrated EDS engine models.
- Completed Step 3 - Generated and evaluated takeoff and approach profiles and quantified deviations.
- Step 4 in progress - Began development and refinement of the BWB ACA model.

## Major Accomplishments

- Developed internal tooling to streamline and make future comparative analyses between EDS and AEDT models more efficient.
- Identified and corrected significant discrepancies in engine rating and thrust modeling between EDS and AEDT and successfully validated the pipeline by generating and evaluating 18 takeoff trajectories and approach profiles.

## Publications

- Tan, Y. T., Kondur, N., Zurtia, F., Xie, J., Cai, Y., Kirby, M., & Mavris, D. (2026, June 8-12). *Development of Advanced Concept Aircraft Model in Aviation Environmental Design Tool*. Submitted to AIAA Aviation 2026 Forum.

## Outreach Efforts

- Attended ASCENT meetings.

## Awards

None.

## Student Involvement

This task involves three graduate students: Yaw Tung Tan, Nina Kondur, and Felipe Zurita

## Plans for Next Period

- Complete the current EDS runs for the BWB and once finalized, process this model through the validated data pipeline to generate the full set of AEDT performance, noise, and emissions coefficients.
- Replicate the trajectory analysis performed in Step 3 using the BWB model. A comprehensive set of departure and approach profiles will be run comparing both EDS and AEDT.
- Upon successful validation, the BWB model will be ready for use in the AEDT, fully enabling the new ACA modeling capability.

# Task 2 - Alternative Design Approaches to Meet Demand

**Georgia Institute of Technology**

## Objective

The objective of this task is to achieve, quantify, and enhance the potential efficiency of next-generation tube-and-wing large single-aisle vehicles and their fleet-wide operations through mission-based optimization enabled by the addition of operational design parameters as design variables. This goal is centered around not only reduced cruise Mach number and lowered design range as suggested by literature review, analysis of real-world operations, and prior work, but also around increased and variable passenger capacity. This variation of passenger capacity is to be enabled by a parametric fuselage sizing methodology, supporting vehicle-level trade-offs and maintaining same network-wide passenger flux with decreased operations. This work investigates how aircraft performance, vehicle-level fuel and noise emissions, and fleet-level environmental outcomes change when a clean-sheet single-aisle aircraft is sized and optimized simultaneously over sequential steps of future technology integration, fixed cruise speed, cruise speed optimization, laminar flow technology infusion, and finally coupled design range and payload capacity variation. These impacts are assessed with fleet-level simulations and comparisons to real-life data obtained from flown missions, as passenger demand evolves to imply a developing need for higher-capacity transports.

To support this objective, the EDS will be used to develop and optimize a family of next-generation single-aisle aircraft, modeling and incorporating technologies expected to achieve deployment readiness by 2035 targeting fuel burn and noise mitigation. The previously developed methodology to capture the natural laminar flow (NLF) aerodynamics and their impact will continue to be utilized, while simultaneously developing a brand-new payload-driven parametric fuselage sizing capability. These vehicles will be evaluated over a broad design space to characterize feasibility boundaries for each design and constraint, design variable impacts, trends which support the optimal design for each payload-range combination, and trade-offs among speed, range, and passenger capacity. The optimized vehicle set will then form the basis for the fleet-level impact study, where the associated reductions in fuel burn and emissions will be quantified. This fleet analysis will evaluate how shorter design ranges yield more efficient vehicles at the expense of reduced operational coverage, and how increased passenger capacity can lower the number of required operations. Particular emphasis will be placed on the fleet-level fuel-burn savings enabled by higher-capacity aircraft through operation count reduction, as well as on the resulting trade-offs between vehicle- and fleet-level outcomes.

The outcomes of this task are expected to first include the development and integration of a parametric and payload-driven fuselage sizing method. The payload-driven fuselage sizing method will enable a quantified understanding of the

impacts associated with the newly added variable of passenger count alongside other aspects of mission-based operational optimization, at both vehicle and fleet levels. Benefits, interdependencies, and trade-offs associated with this study aim to inform realistic performance targets as supported by technology development, production, and entry-into-service scenarios for future single-aisle aircraft. This group aims to refine previous work, further developing assumptions for market share evolution and impact of vehicles with different operational goals, environmental targets, and potential increased efficiency of next-generation conventional configurations.

## Research Approach

The methodology applied in this research task builds upon the framework originally developed for the Long-Term $CO_x$ Aspiration Goals (LTAG) study conducted by Committee on Aviation Environmental Protection (CAEP) in International Civil Aviation Organization (ICAO), which was conducted by Georgia Tech in support of the FAA, The present work extends that framework to incorporate (i) updated 2035 technology forecasts with a larger technology portfolio, (ii) improved fuselage sizing formulations that enable parametric variation in passenger capacity, and (iii) an expanded design space including variations in design range, cruise Mach number, and payload (passenger) capacity. These enhancements support a more comprehensive evaluation of how mission-optimized single-aisle aircraft affect vehicle-level performance and fleet-wide environmental and operational outcomes. The major steps of the analysis are summarized in Figure 9 and are described below.

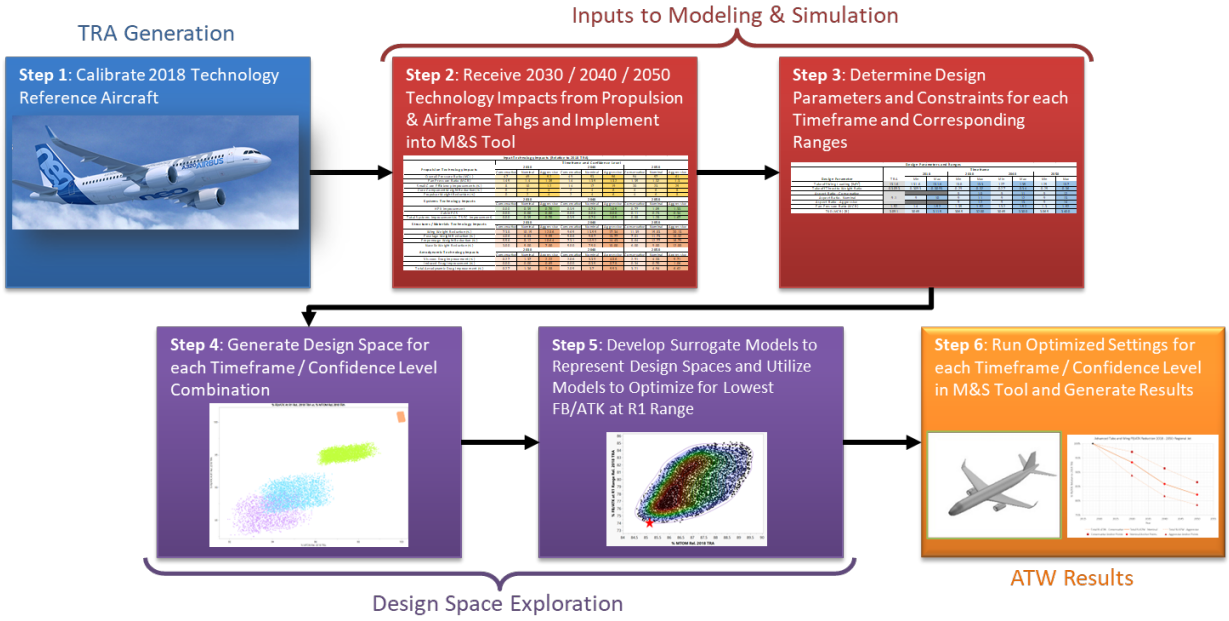


**Figure 9.** Long-term aspirational goal (LTAG) advanced tube and wing aircraft assessment method. ATW: Advanced Tube and Wing, FB/ATK: Fuel Burn per Available Tonne-Kilometer, M&S: modeling and simulation.

**Step 1 - Technology Reference Aircraft Generation**

The TRA represents the present-day state-of-the-art baseline against which the impacts of future technology and design changes are evaluated. As in prior work, a notional Airbus A320neo equipped with PW1127G geared turbofan engines is modeled in the EDS modeling and simulation environment, consistent with the 2018 narrow-body reference used during the LTAG study. Updates include refined calibrations of noise performance and takeoff/landing field lengths, while the key specifications are summarized in Table 3. Beyond being the vehicle-level reference point, the TRA also serves as the business-as-usual comparator for subsequent fleet-level analyses.

**Table 3.** Key design specifications of the TRA model.

| Parameter | Unit | Value |
|---|---|---|
| **Number of passengers** | – | 150 |
| **Design range** | nm | 3,420 |
| **Cruise Mach number** | – | 0.78 |
| **Maximum cruise altitude** | ft | 41,000 |
| **Maximum ramp weight** | lb | 175,047 |
| **Maximum sea-level static thrust** | lb | 2 × 27,080 |
| **Reference wing area** | $ft^2$ | 1,341 |
| **Wingspan** | ft | 112.8 |
| **Takeoff field length** | ft | 6,619 |
| **Landing field length** | ft | 6,512 |

**Step 2 - 2035 Technology Modeling**

Consistent with the forecasts for the maturing airframe, propulsion, and noise reduction technologies, as well as the approximately two-decade service introduction cycles between generations of designs, the next-generation successor to the A320neo is assumed to enter service in 2035, incorporating technologies that have matured by this point. This date reflects the expected readiness of major aerodynamic, structural, propulsive, and acoustic technologies, justifying the engineering effort for a clean-sheet design. In addition, 2035 represents a plausible entry-in-service (EIS) date allowing propagation across the market to enable meeting international environmental goals such as net-zero 2050 initiatives. The 2035 technology portfolio draws from two sources: the ICAO LTAG Technology Subgroup Review, which provides 2030 and 2040 medium-confidence estimates for propulsion, structural, and aerodynamic technology impacts, and the ICAO Independent Expert Integrated Review (IEIR) Noise Technology Review, which provides predicted 2027 and 2037 noise mitigation impacts, both interpolated to obtain 2035 technology impacts. For a conservative estimation, only the moderate confidence of the LTAG and IEIR technology forecasts is utilized. The impacts of integrating technologies on the TRA model are summarized in Table 4. These impacts represent improvements in key design and performance parameters due to the expected evolution of technologies through research and development. The propulsion system of the 2035 design remains the geared turbofan engine, but along with the advanced cycle design, new engine components built with new materials and improved manufacturing processes are expected to improve overall engine efficiency and reduce engine weight. The structural technologies mainly include innovative composite materials and their associated manufacturing processes to decrease the weights of aircraft structural components. The drag reductions introduced by aerodynamic technologies are mainly due to the advanced aerodynamic shape optimization. Noise technologies focus on mitigating the airframe noise, particularly from high-lift devices and landing gears, as well as core and fan noise from engines.

**Table 4.** Impacts of 2035 technologies on the TRA model.

| Technology Impact | Improvement |
|---|---|
| **Engine core component weight** | -3.00% |
| **Fan efficiency** | +0.95% |
| **Low-pressure compressor (LPC) efficiency** | +1.15% |
| **High-pressure compressor (HPC) efficiency** | +1.96% |
| **High-pressure turbine (HPT) efficiency** | +0.95% |
| **Low-pressure turbine (LPT) efficiency** | +1.21% |
| **Reduction in small core efficiency losses** | +13.50% |
| **TSFC improvement from power extraction** | -0.53% |
| **Wing weight** | -11.85% |
| **Fuselage weight** | -8.35% |
| **Empennage weight** | -9.52% |
| **Nacelle weight** | -6.25% |
| **Lift-independent drag** | -2.38% |
| **Lift-dependent drag** | -0.18% |
| **Jet noise** | -0.80% |
| **Inlet noise** | -2.39% |
| **Fan discharge noise** | -3.02% |
| **Core (combustor) noise** | -6.00% |
| **Turbine noise** | -2.00% |
| **Landing gear noise** | -3.60% |
| **Trailing edge flap noise** | -2.80% |
| **Leading edge flap noise** | -16.60% |

Aside from the technologies listed above, the reduction of cruise speed also provides an opportunity for NLF technology integration. NLF reduces aircraft skin friction drag by shaping the airfoil to delay boundary layer transition from laminar to turbulent. When the cruise speed reduces from the transonic to subsonic regime, wave drag decreases, and skin friction drag becomes the dominating factor, creating a need to decrease skin friction drag for better aerodynamic efficiency. Simultaneously, a lower sweep angle may become feasible as wave drag decreases, which discourages crossflow instability and supports the implementation of NLF.

Instead of modeling the skin friction drag reduction due to the NLF as a constant, this research improves the NLF modeling approach of the LTAG study by incorporating additional influencing factors, including the Mach number, Reynolds number, and sweep angle. Specifically, in this task, the NLF is modeled using the flat plate approximation and analyzed using NASA's aircraft design tool FLOPS. The percentage of the laminar region on the wing surface is computed as the ratio between the transition Reynolds number and the local Reynolds numbers at different spanwise locations. The local Reynolds numbers are computed based on the altitude, Mach number, and local chord lengths, whereas the transition Reynolds number is determined by the leading-edge sweep angle using the crossflow instability and the Tollmien-Schlichting instability theories. The regions enclosed by control surfaces, behind the nacelles, and near the fuselage are assumed turbulent because of large disturbances.

The proposed NLF modeling method was applied to NASA's Common Research Model (CRM)-NLF model for validation. The calculated percentage of the laminar region on the wing was compared to the experimental result documented in the literature. Figure 10 shows the laminar area computed for the CRM-NLF model using the proposed method. The Mach

number and Reynolds number of the validation case are at 0.86 and $1.5 \times 10^7$, respectively. The upper surface laminar portion calculated by the proposed model is 55.6%, which closely aligns with the experimental result of 56.0%. The cruise lift-to-drag ratio improvement was also compared between two sides, with the proposed model result of 6.87% consistent with the experimental result of 6.81%.

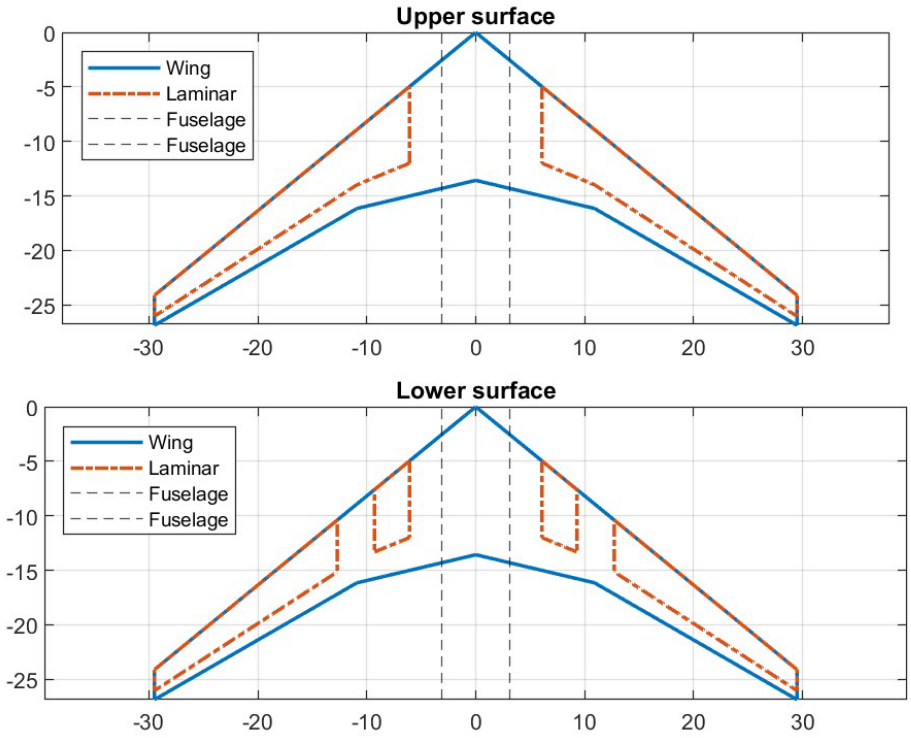


**Figure 10.** Laminar region on the wing surfaces of the Common Research Model-Natural Laminar Flow (CRM-NLF) model.

**Step 3 – Fuselage and Cabin Sizing Method**

To support the inclusion of passenger capacity as a design variable in the design space exploration for next-generation transports, a new fuselage sizing method with parametric variation of fuselage dimensions as a function of user-input payload capacity was required to replace the FLOPS methods constructed using legacy data. During this task, two new fuselage sizing methods were developed. The first mimicked the method used in FLOPS, estimating fuselage dimensions through a build-up of cabin elements based on physical dimensions called the Detailed-Layout Based Method, and a second, simplified, regressions-based model called the Data-Driven Direct Sizing Method. The first method reconstructs cabin geometry using physical dimensions and numbers of galleys, lavatories, doors, and effective joint lengths for all based on the number of passengers and number of seats abreast. While defining the seat pitch for the various classes ultimately helps with the prediction, the method is even able to assume default values and seat density, operating with a minimal number of inputs, requiring only counts of tourist and first-class passengers. Alternatively, the second method computes the counts of cabin elements after directly sizing the fuselage, and only for reference purposes. This data-driven method sizes the fuselage based on various regressions and relations between passenger compartment and fuselage dimensions with the passenger counts per class. While both methods have been made compatible with the modeling and simulation tool EDS, specifically through the input design of experiments, ultimately the latter method was selected due to its simplicity and lower computational cost. Regardless, both methods exhibited promising predictive performance, especially for the narrow-body passenger range between 130 and 270, with the percent error accuracy of both methods displayed in Figure 11 and Figure 12.

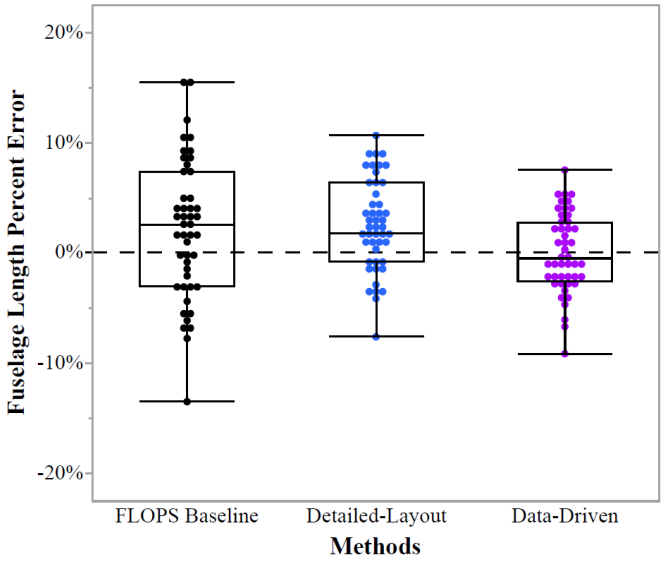


**Figure 11.** Comparison of fuselage length approximation between baseline and proposed methods. FLOPS: Flight Optimization System.

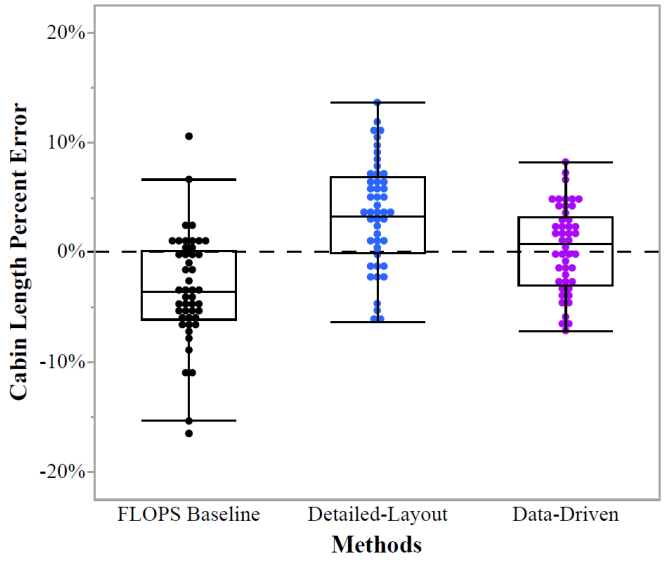


**Figure 12.** Comparison of cabin length estimation between baseline and proposed methods. FLOPS: Flight Optimization System.

**Step 4 - Design Space Exploration**

The design space of interest is constructed by the design variables and their associated ranges shown in Table 5. Aside from the variables used in the LTAG study, additional wing geometric parameters are added to the design space to maximize the benefits of reducing cruise speed and design range. The design objective is to minimize the block fuel of the design mission. The constraints considered in the optimization are summarized below:

- Takeoff field length at maximum takeoff weight (MTOW) and sea-level International Standard Atmosphere (ISA) condition no longer than 6,619 ft
- Landing field length at maximum landing weight and sea-level ISA condition no longer than 6,512 ft
- Wingspan no longer than 118 ft (Aircraft Design Group III)
- Excess fuel capacity for the design mission must be non-negative
- Fan diameter no greater than 86.04 ft
- Core size parameter no lower than 2.8 lb/s
- Maximum high-pressure compressor temperature no higher than 1,800° R

**Table 5.** Design variables and ranges. TRA: Technology Reference Aircraft.

| Design Variable | Timeframe | | |
|---|---|---|---|
| | TRA | 2035 | |
| | | Minimum | Maximum |
| **Design range (nm)** | 3,420 | 1,500 | 3,420 |
| **Cruise Mach number** | 0.78 | 0.70 | 0.80 |
| **Thrust-to-weight ratio** | 0.31 | 0.28 | 0.33 |
| **Wing loading (lb/ft$^2$)** | 131 | 128 | 134 |
| **Fan pressure ratio** | 1.52 | 1.375 | 1.55 |
| **Overall pressure ratio** | 45.8 | 41 | 51 |
| **Maximum turbine entry temperature (R)** | 3,360 | 3,334 | 3,519 |
| **Extraction Ratio** | 1.128 | 0.95 | 1.25 |
| **Wing aspect ratio** | 9.5 | 7.5 | 11.5 |
| **Wing taper ratio** | 0.19 | 0.15 | 0.25 |
| **Wing average thickness to chord** | 0.138 | 0.1 | 0.14 |
| **Wing quarter-chord sweep angle (°)** | 25.3 | 15 | 27 |

The first three constraints ensure the new aircraft maintains compatibility with all existing airport facilities. The fan diameter constraint ensures ground clearance of the nacelles. The last two constraints ensure the high-pressure compressor is manufacturable and its operating temperature does not exceed material temperature limits.

To sample the design space, nearly 20,000 DoE cases are generated using the design variables and their ranges listed in Table 4 by applying Box-Behnken and Face-Centered Central Composite designs to sample edge cases, with the Latin hypercube design applied for interior design space sampling. This DoE is run through the EDS design environment twice with two settings: (1) the NLF model disabled and (2) the NLF model activated, resulting in nearly 40,000 total cases. Based on the responses of the sampling cases, surrogate models are established between metrics of interest (i.e., design objective and constraints) and design variables using two-layer neural networks. To ensure that the established surrogate models are sufficiently accurate to replace true functions, multiple validation metrics are evaluated, including $R^2$, the root mean squared error, the actual versus predicted plot, and the residual versus predicted plot. Using these surrogate models, a set of constrained optimizations is performed to obtain optimal designs for varying scenarios, and these designs are then re-evaluated in EDS to determine fuel burn improvements.

**Step 5 - Fleet-Level Impact Evaluation**

The fleet analysis is performed using the in-house tool Global and Regional Environmental Aviation Trade-Off (GREAT). In GREAT, all aircraft are categorized into seat classes based on their passenger capacities. These seat classes include short thin haul (SHT), small regional jet (RJ-S), large regional jet (RJ-L), turboprop (TP), small single aisle (SSA), large single aisle (LSA), small twin aisle (STA), large twin aisle (LTA), and very large aircraft (VLA). The evaluation of the fleet composition depends on the retirement of old aircraft and subsequent replacement with new aircraft. Each seat class in GREAT is modeled using a retirement curve derived from historical data. Replacements are modeled using a structure matrix considering three aspects: (1) aircraft age, prioritizing the oldest units first, (2) mission capabilities, and (3) environmental feasibility. Meanwhile, the new aircraft's capabilities with respect to the design range, payload, and seat class must be equal to or greater than those of the previous aircraft that it is replacing. Finally, the fuel burn or emissions produced by this aircraft must be improved compared to those of the older aircraft. Figure 13 depicts the retirement and replacement algorithm used in GREAT.

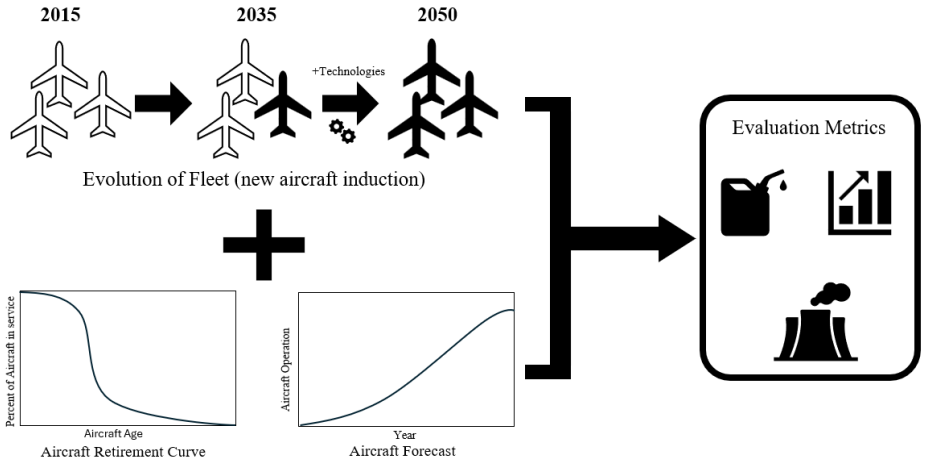


**Figure 13.** Retirement and replacement algorithm in GREAT.

The forecast model of the future flight demands integrated in GREAT is established based on the Boeing Commercial Market Outlook (CMO). As shown in Figure 14, this forecast model includes the COVID years and provides information on the forecasted recovery of air travel demand in post-COVID years. The black curve in the plot represents the growth in total operations from 2015 to 2050. Note that since the Boeing CMO only predicts the operations until 2041, the growth rates between 2041 and 2050 are based on extrapolation. The colored bars in Figure 14 denote the percentage of total operations covered by different classes of aircraft. For each class, the shaded bar represents the aircraft that are out of production, while the bright bar represents the aircraft that are still in production.

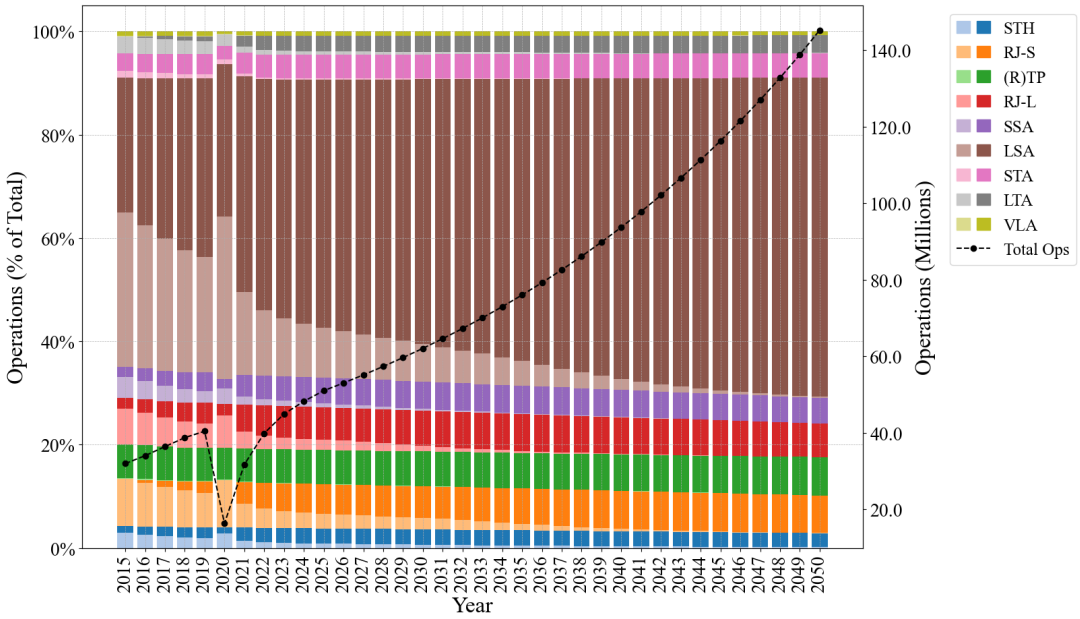


**Figure 14.** Commercial aviation growth forecast and business-as-usual scenario.

Although reducing the design range lowers an aircraft's fuel consumption due to a smaller vehicle size and lower thrust requirement, it also limits the set of missions the aircraft can serve. To assess how this constraint affects the fleet operation, this task performs a fleet analysis built upon the design space exploration results obtained from Step 4. Assuming the optimal designs with reduced design range, optimized cruise speed, and increased passenger capacity begin replacing the previous generation single-aisle aircraft in the current fleet starting from 2035, multiple fleet evolution scenarios are analyzed. To reflect a realistic EIS profile, a 6-year ramp-up schedule is applied, increasing the production share of the new vehicle from 0% to 100% between 2034 and 2039. This approach captures an initially slow rollout, accelerated production as manufacturing stabilizes, and tapers to full-scale class-wide production at full demand levels. Because the short-range optimized vehicles are unable to serve all mission ranges, longer missions within the same seat-class continue to be operated by the baseline TRA. As payload capacity is now a design variable in the vehicle optimization process, the fleet replacement logic is updated to reflect changes in the number of operations required to transport the same passenger demand. When aircraft with higher seating capacity enter the fleet, the required number of operations is reduced accordingly. Two adjustment approaches are applied, with the latter introducing a "penalty factor" to better represent operational realities, such as the occasional need for additional flights to satisfy the demand distribution across various hours of the day. These are:

- Option 1: Direct proportional scaling based solely on the ratio of the original to increased passenger capacity, preserving total transported passengers.

$$N_{\text{adj},1} = \frac{PAX_{\text{orig}}}{PAX_{\text{inc}}} N_{\text{orig}} \qquad \text{(Eq. 1)}$$

- Option 2: A moderated adjustment that partially reverses the capacity-based scaling to account for operational realities such as variable load factors and scheduling flexibility.

$$N_{\text{adj},2} = N_{\text{adj},1}\left[1 + p\left(1 - \frac{PAX_{\text{orig}}}{PAX_{\text{inc}}}\right)\right] \qquad \text{(Eq. 2)}$$

These adjusted operation counts directly modify the replacement percentages applied within GREAT. Higher-capacity aircraft receive lower replacement shares under both options, with Option 2 producing slightly higher values due to its more conservative treatment of operational efficiency gains. In this task, a baseline "business-as-usual" scenario is first established, followed by 50 scenarios using the optimized vehicles replacing the existing fleet, as summarized in Table 6.

In the baseline scenario, no newly designed aircraft is introduced, and the industry maintains production of existing vehicles with anticipated annual market and operations growth, intended to represent the current real-world situation. The scenario includes cases such as waiting until novel concept programs come to fruition or new vehicles arriving to the market with EIS dates following 2035. It could also represent new models being introduced in the fleet being less impactful. Fifty other scenarios were sketched to utilize the findings of the vehicle design study and its corresponding resultant optimized vehicle. The 51 scenarios are executed twice in GREAT, where the first execution uses Option 1 and the second uses Option 2 with a penalty factor of $p = 0.25$.

**Table 6.** Vehicle production and replacement scenarios of consideration. ATA: Advanced Technology Aircraft, LSA: large single aisle, SSA: small single aisle.

| Scenario | Optimized Aircraft | Design Range (nm) | Replaced Aircraft Class |
|---|---|---|---|
| 1 | Business as usual | | |
| 2-6 | ATA 1-5 | 1,500 | LSA only |
| 7-11 | ATA 6-10 | 1,700 | LSA only |
| 12-15 | ATA 11-14 | 2,000 | LSA only |
| 16-19 | ATA 15-18 | 2,500 | LSA only |
| 20-23 | ATA 19-22 | 3,000 | LSA only |
| 24-26 | ATA 23-25 | 3,420 | LSA only |
| 27-31 | ATA 1-5 | 1,500 | LSA and SSA |
| 32-36 | ATA 6-10 | 1,700 | LSA and SSA |
| 37-40 | ATA 11-14 | 2,000 | LSA and SSA |
| 41-44 | ATA 15-18 | 2,500 | LSA and SSA |
| 45-48 | ATA 19-22 | 3,000 | LSA and SSA |
| 49-51 | ATA 23-25 | 3,420 | LSA and SSA |

The outputs from the tool include total operations conducted by that aircraft, annual distance covered, fuel burn, and carbon and nitrogen oxides ($NO_x$) emissions. To evaluate the global impact induced by the introduction of newly designed vehicles compared to the non-replacement scenario, these metrics are added up for the particular seat class and plotted against the time period in consideration.

## Milestones

- Developed a fully parametric, payload-driven fuselage and cabin sizing methodology, replacing the legacy FLOPS formulations with two models: a data-driven direct estimation, and a physical dimensions-based detailed-layout buildup of components, scalable from smallest single-aisle to largest twin-aisle configurations.
- Validated the new fuselage sizing methodology using a comprehensive set of real aircraft data and comparing the performance with other legacy and modern tools with fuselage sizing capabilities, including FLOPS, SUAVE[2], Aviary/GASP[3], as well as established published regression-based sources like Roskam and Raymer, demonstrating improved accuracy and robustness across all classes.
- In the process of publishing a conference proceeding to 2026 SciTech titled "Rapid Fuselage and Cabin Sizing Method for Commercial Transport Aircraft Design," documenting the performance and results of the proposed fuselage and cabin sizing methods, alongside comparison with existing literature and tools.
- Completed identification, modeling, and infusion of 2035 propulsion, structural, aerodynamic, and acoustic technologies from ICAO LTAG and IEIR technology portfolios, as well as NLF aerodynamic model, achieving ATA model.

[2] SUAVE is a conceptual level aircraft design environment built with the ability to analyze and optimize both conventional and unconventional designs. SUAVE is a development of the Stanford Aerospace Design Lab.
[3] Aviary/GASP is NASA's aircraft analysis, design, and optimization tool.

- Performed a comprehensive design space exploration using EDS, densely sampling the design space with nearly 40,000 samples, obtaining responses of metrics and constraints of interest, followed by establishing high-accuracy neural net surrogate models to characterize the responses as functions of design variables, enabling optimization.
- Performed mission-based optimization across an array of payload-range design points, identifying feasible configurations, determining active constraints, and generating conceptual aircraft models for all viable combinations, while also re-performing past year setup, configuration, and results for crosscheck and validation.
- Investigated relaxation of constraints to obtain feasible designs across all design combinations.
- Developed setup and approach enhancements to the GREAT fleet analysis framework to accommodate variable passenger capacity and analysis of its influence on operations, replacements, and mission feasibility.
- Established and evaluated all-new fleet replacement scenarios, selected specifically to characterize distinct and joint effects of reduced range decreasing operational coverage and increasing passenger capacity transporting equal number of passengers in less operations, incorporating payload-dependent operations scaling, nonlinear fleet introduction ramp-up, and range-bounded mission assignments for range-limited vehicles.
- Visualized the results of vehicle and fleet-level analyses, displaying impacts across fuel burn, operations, noise, and comparing new optimized vehicles against business-as-usual baselines.
- In the process of publishing vehicle and fleet-level results as two separate but companion conference proceedings in 2026 Aviation, titled “Assessing Impacts of Design Range and Payload on Next-Generation Single-Aisle Transport Fuel Burn and Noise” and “Fleet-Level Assessment of Mission-Optimized Next-Generation Single-Aisle Aircraft with Varying Payload,” documenting the methodology, results, and implications.

## Major Accomplishments

This task has delivered a two-part major accomplishment, with one part being the optimized 2035 single-aisle aircraft designs with reduced cruise speeds at multiple design ranges, and the other being fleet-level fuel burn impacts of introducing these optimized designs into fleet operations.

**Part 1 - Vehicle-Level Assessment**

Figure 15 illustrates the sequential reduction in block fuel achieved in each stage of the optimization process. Integration of 2035 LTAG technologies provides the single largest improvement, reducing fuel weight by about 12% for each range considered, as depicted by the blue bars. Fixed-speed optimization at a cruise speed of Mach 0.78 contributes further 7-8% block fuel reductions, as shown by the orange bars. Adding optimization of the cruise speed, shown by the gray bars, further reduces fuel consumption by approximately 2%. Lastly, the integration of NLF technologies and corresponding vehicle resizing, as seen in the purple bars, yields an additional block fuel reduction of about 6% across all the ranges analyzed.

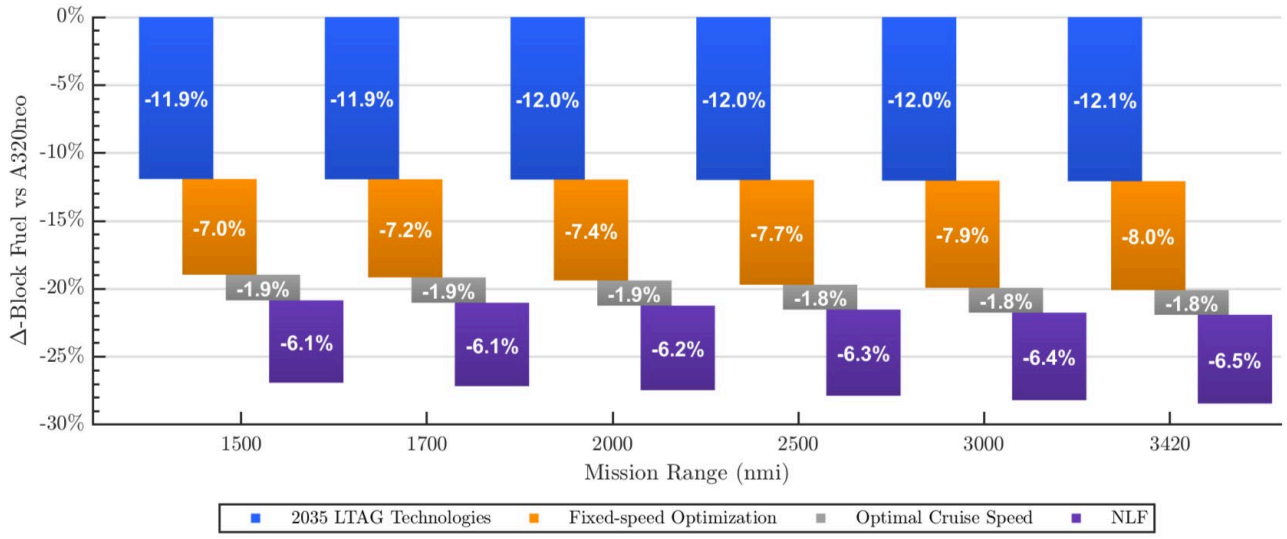


**Figure 15.** Block fuel reduction progression through sequential optimization process. LTAG: Long-term aspirational goal, NLF: natural laminar flow.

Figure 16 shows the resulting block fuel reductions across all range-payload combinations considered. Significant reductions of around 30% in block fuel weight are exhibited across all ranges for 150 passenger configurations, with the greatest reduction occurring with the lowest range of 1,500 nmi. The configurations at the upper limits of passenger capacity and range could not satisfy all design constraints and were subsequently omitted. Figure 17 presents the corresponding improvements in fuel-per-passenger-mile of optimized candidate vehicles; this figure was constructed to facilitate a direct comparison of the 150 passenger-3,420 nmi range TRA baseline with the final optimized vehicles. A region of desirability is displayed for combinations of increased passenger counts and reduced design ranges from that of the TRA baseline, with the greatest efficiency improvement of 35.8% shown by the 190 passenger-1,500 nmi model.

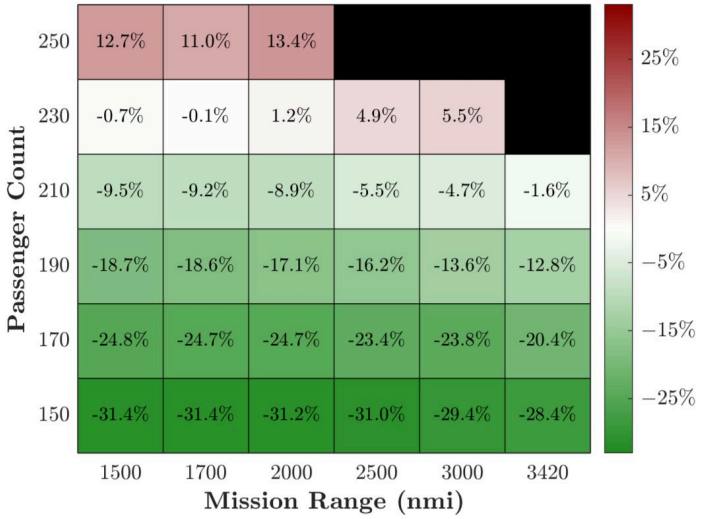


**Figure 16.** Block fuel reductions of optimized designs sized with respect to various combinations of design ranges and payloads compared to 150-pax TRA baseline.

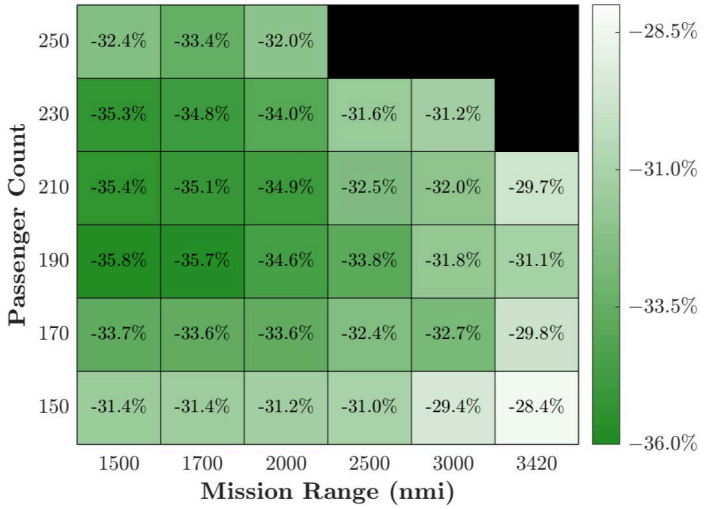


**Figure 17.** Fuel-per-passenger-nautical-mile reductions with respect to the 150-pax TRA baseline vehicle.

With a similar step-by-step optimization process, optimized vehicles for cumulative noise minimization were also produced. Figure 18 illustrates the cumulative noise reductions achieved, the greatest magnitude reduction stemming from integration of 2035 LTAG technologies, which reduce cumulative noise levels across the three certification recording locations by 9.0 effective perceived noise in decibels (EPNdB). Resizing the candidate vehicle with airframe and engine cycle design variables optimized reduces the cumulative noise by a further 6.4 EPNdB. Adding optimization of cruise speed alongside aircraft resizing delivers a more modest reduction of cumulative noise by 1.3 EPNdB, while NLF technology integration delivers a minute reduction of 0.1 EPNdB as turbulent airflow over lifting surfaces is deterred.

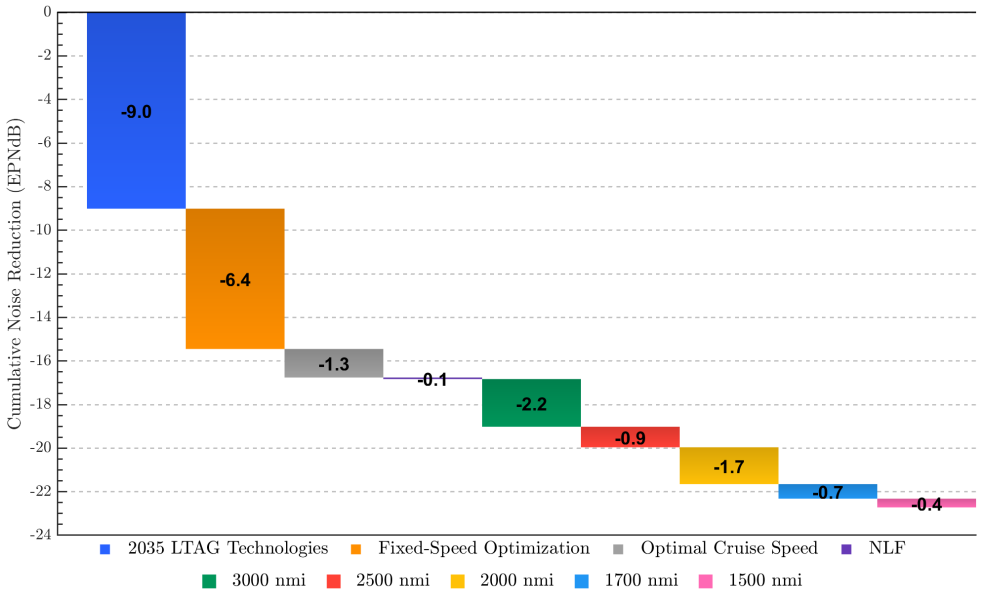


**Figure 18.** Cumulative noise reduction progression through sequential optimization process.

**Part 2 - Fleet-Level Assessment**

The 51 scenarios were executed twice, resulting in two sets of results corresponding to the two options of adjusting the number of operations. These options differ in whether a penalty factor is applied to simulate realistic daily schedule

demand. Option 1 represents an optimistic case in which the number of operations decreases directly in proportion to the increase in passenger capacity while maintaining baseline passenger flux. Alternatively, Option 2 includes a relatively harsh operations penalty, reflecting the operational reality that additional flights may be required to meet demand patterns, with the reality likely to fall between these scenarios. Figure 19 shows the implementation of Options 1 and 2 for increasing passenger count. The replacement percentages for 150-passenger aircraft align with the baseline as capacity remains unchanged. As passenger capacity increases, replacement percentages decrease relative to the baseline, but when Option 2 is enabled, some of the reduced replacement percentage is reverted, with the differential between Options 1 and 2 expanding as passenger capacity increases. The delta between the two options is 0% for 150 passenger configurations, about 5% for 175 passengers, and nearly 20% for the 250 passenger configurations. Option 1 yields lower replacement percentages, while option 2 produces slightly higher values by accounting for operational and scheduling needs.

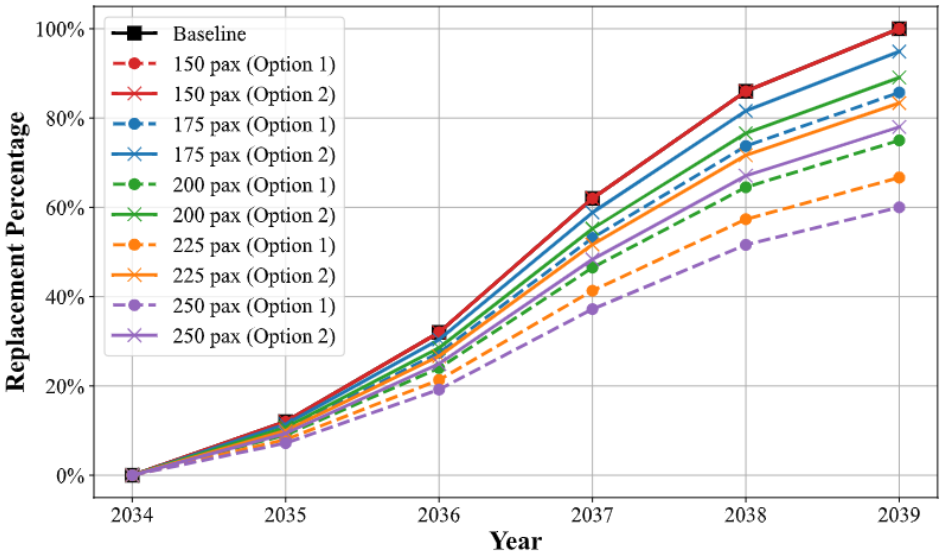


**Figure 19.** Operation replacement percentages for different passenger capacities.

The environmental benefits of introducing optimized aircraft to global fleets were evaluated through cumulative fuel-burn impacts for LSA, SSA, and global fleets across all replacement scenarios. The first set of figures portray the fuel burn changes when optimized vehicles replace only the LSA class. The second set portrays the changes when optimized vehicles replace both LSA and SSA classes, where the LSA fleet fuel burn changes are plotted with solid lines and the SSA fleet changes are plotted in dashed lines. The third set shows the global change for two replacement assumptions, with the solid lines representing only the LSA class being replaced, and the dashed lines showing both LSA and SSA classes being replaced.

In Figure 20 and Figure 21, two clear patterns are visible. The first is that the benefits of LSA-class fuel burn reduction, which would also be global as no other vehicle is being replaced, peak at 2,000 nmi for both the penalized and penalty-free options when passenger count is increased. The previous year's results showed that benefits for 2,000 nmi and 2,500 nmi vehicles were nearly identical, with the latter only slightly greater. However, those results were evaluated only at the 150-passenger size, included here as well. When passenger count is increased, the 2,000 nmi vehicle shows a greater benefit. With Option 1, the vehicle optimized for a 2,000 nmi and 200 passenger design mission shows the greatest benefit of about 16.8%. The second observation is that the penalty factor impacts the higher passenger capacity vehicles to a greater degree, and as the passenger count increases, the benefit loss deteriorates. At $p = 0.25$, this results in the new best-performing vehicle being optimized for a 2,000 nmi and 175 passenger design mission. When $p$ increases, the passenger capacity of the optimal design lowers as the benefit of increasing passenger count diminishes, as the negative impact of operating a larger vehicle remains, while the benefit of operating fewer missions becomes less potent.

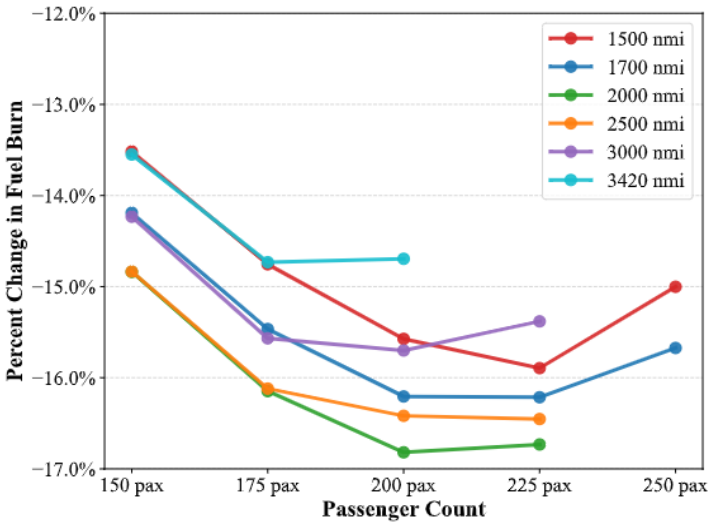


**Figure 20.** Cumulative LSA fleet fuel-burn reduction compared to the baseline scenario (Option 1, no penalty factor)

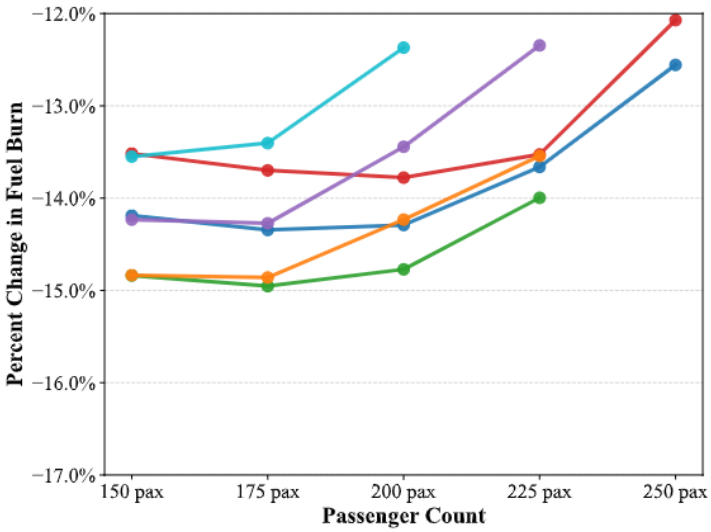


**Figure 21.** Cumulative LSA fleet fuel-burn reduction compared to the baseline scenario (Option 2, $p = 0.25$)

Then, when both LSA and SSA vehicles are replaced by the new designs, new insights arise from the impact within the SSA class and its differentiation from LSA trends, as shown in Figure 22 and Figure 23. As SSA vehicles are smaller than LSA vehicles, introducing higher-capacity designs yield an even stronger effect. Equal passenger flux can be met with substantially fewer operations, amplifying fleet-level benefits. Consequently, the best-performing optimized design shifts toward larger-capacity designs. In Figure 23, it can be seen that SSA-class benefits maximize with a passenger count of 225 for ranges of 1,500, 1,700, 2,000, and 2,500 nmi, with 1,500 nmi displaying the greatest improvement, achieving a nearly 22% SSA-class fuel burn reduction. However, this strong influence of payload capacity also increases the effect of the penalty factor. When the penalty factor is applied, the optimal point shifts significantly to the 175-passenger, 2,000-nmi design, indicating the greater operational penalties imposed on very high-capacity aircraft.

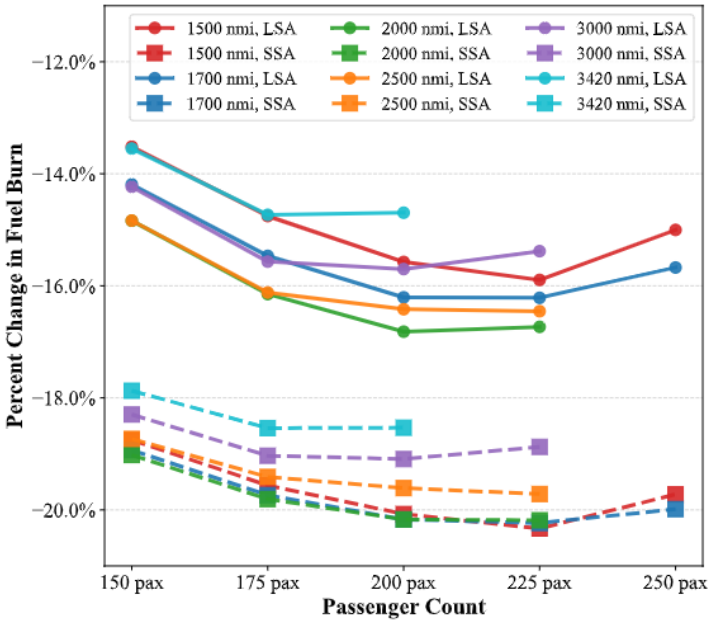


**Figure 22.** Cumulative large single aisle (LSA) and small single aisle (SSA) fleet fuel-burn reductions compared to baseline (Option 1, no penalty factor).

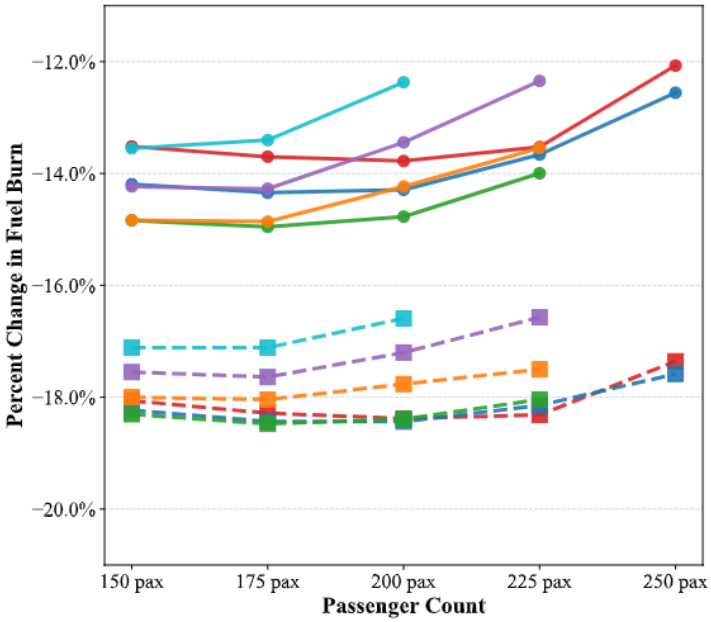


**Figure 23.** Cumulative large single aisle (LSA) and small single aisle (SSA) fleet fuel-burn reductions compared to baseline (Option 2, $p = 0.25$).

Lastly, the global fuel burn reduction is evaluated across all seat classes, comparing scenarios with and without SSA replacement and using both operational adjustment options. The results are provided in Figure 24 and Figure 25. Under

Option 1, the maximum fuel burn reduction is approximately 7.0% when replacing LSA aircraft only, and 7.6% when replacing both LSA and SSA, with the optimal point occurring at 200-passenger, 2,000-nmi vehicle. This outcome aligns with expectations. Although SSA benefits slightly more from higher-capacity designs, the LSA class dominates the market, so that global optimum closely follows the LSA trend. A similar pattern appears under Option 2, where the optimal design shifts to the 175-passenger, 2,000-nmi vehicles. This shift is again driven primarily by LSA class, while the imposed penalty factor reduces the overall benefit, yielding a maximum fuel burn reduction of about 6.8%.

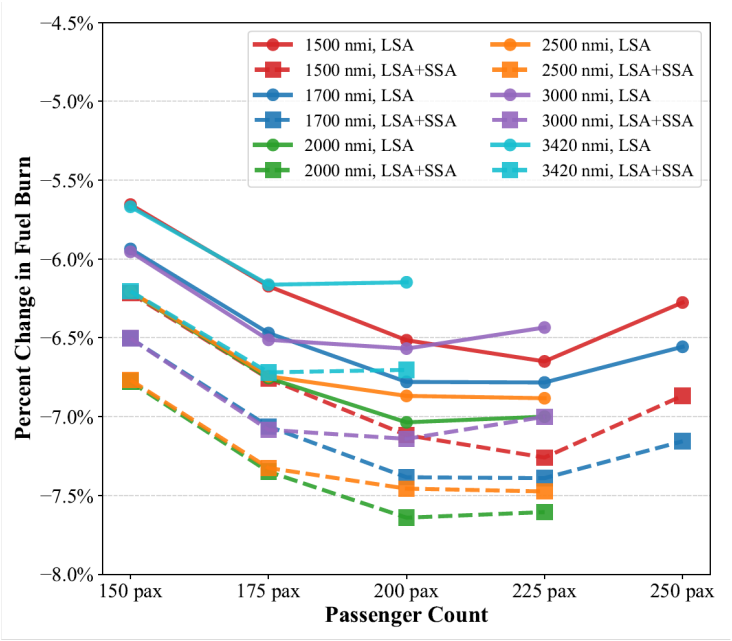


**Figure 24.** Global fuel burn reduction compared to baseline scenario (option 1, no penalty factor). LSA: large single aisle, SSA: small single aisle.

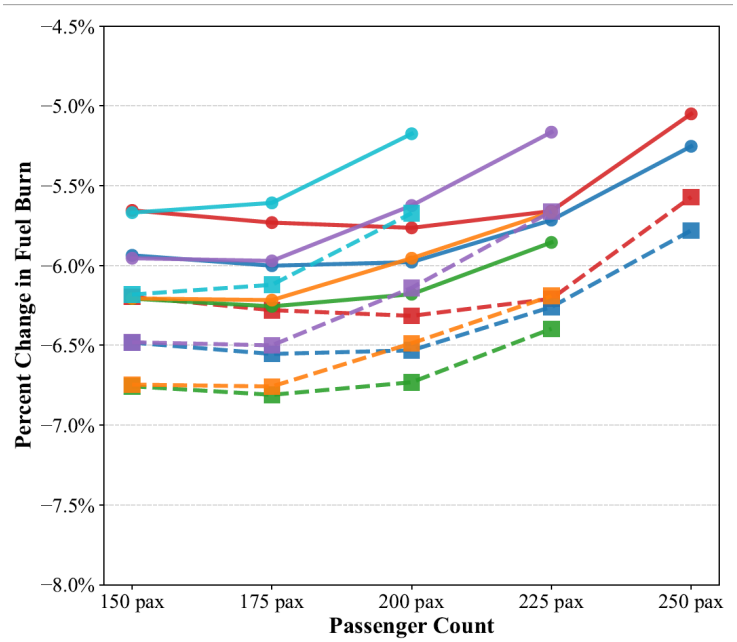


**Figure 25.** Global fuel burn reduction compared to baseline scenario (option 2, $p = 0.25$). ). LSA: large single aisle, SSA: small single aisle.

## Publications

### Journal Article

Ergan, T., Parashar, A., Xie, J., Cai, Y., Kirby, M., Gladin, J., & Mavris, D. (in review). Design and Fleet-Level Assessment of Next-Generation Single-Aisle Aircraft with Reduced Range and Cruise Speed. Submitted to *Journal of Aircraft*.

### Conference Proceedings

Cheng, Y., Ergan, T., Xie, J., Kirby, M., Gladin, J., & Mavris, D. (2026, June 8-12). *Fleet-Level Assessment of Mission-Optimized Next-Generation Single-Aisle Aircraft with Varying Payload*. Submitted to AIAA Aviation 2026 Forum.

Cocoves, N., Ergan, T., Benhissoune, S., Cai, Y., Gladin, J., & Mavris, D. (2026, June 8-12). *Assessing Impacts of Design Range and Payload on Next-Generation Single-Aisle Transport Fuel Burn and Noise*. Submitted to AIAA Aviation 2026 Forum

Cheng, Y., Ergan, T., Cocoves, N., Xie, J., Cai, Y., Kirby, M., and Mavris, D. (2026, January 12-16). *Rapid Fuselage and Cabin Sizing Method for Commercial Transport Aircraft Design*. Accepted in AIAA SciTech 2026 Forum. To be published.

Ergan, T., Parashar, A., Xie, J., Kirby, M., & Mavris, D. (2025, January). Fleet-level and global emissions impact analysis of mission-optimized next-generation single-aisle aircraft. *AIAA SciTech 2025 Forum*, AIAA 2025-2168. https://doi.org/10.2514/6.2025-2168

Patel, D., Ergan, T., Cai, Y., Gladin, J., & Mavris, D. (2025, January). Performance assessment and mission-based optimization for next-generation single-aisle aircraft conceptual design. *AIAA SciTech 2025 Forum*, AIAA 2025-0001. https://doi.org/10.2514/6.2025-0001

## Outreach Efforts

- Attended ASCENT biannual meetings.
- Presented Performance assessment and mission-based optimization for next-generation single-aisle aircraft conceptual design and Fleet-level and global emissions impact analysis of mission-optimized next-generation single-aisle aircraft at the AIAA SciTech 2025 Forum, Orlando, Florida (January 6-10, 2025).

## Awards

None.

## Student Involvement

This task involved five graduate students: Tuna Ergan, Yutong Cheng, Nicholas Cocoves, Ty Mancao, and Salma Benhissoune.

## Plans for Next Period

- Update the passenger capacity design points with smaller increments for a denser passenger-range combination array and re-performing both the vehicle-level and fleet-level analysis, as the limited feasibility for high passenger count-high range combinations a limit proper characterization of higher range and payload optima.
- Continue investigating relaxed constraints study, possibly as enabled by other sets of emerging technologies like folding wingtips eliminating wingspan as limiting constraint, with intention of achieving full feasibility across selected design points.
- Expand fleet-level analysis developments to allow comparisons of and across different novel and conventional architectures and configurations to support development-level trade-off studies.
- Investigate incorporation of fleet-level output metrics in the optimization study as part of work towards achieving fleet-informed vehicle design and optimization.

# Task 3 - Exploring Physics-Based Boundaries of the Possible

**Georgia Institute of Technology**

## Objective

The objective of this task is to examine the physics-based limitations of business-as-usual turbofan architecture. This type of study would aid the FAA in understanding the boundaries of the possible, rather than building from a baseline by applying specific individual technologies that benefit efficiency. Depending on any follow-on actions from the LTAG task group analyses, this task may also include the identification of barriers for future ACA and their propulsion systems, or additional supporting analysis.

## Research Approach

**Step 1 - Engine Materials**

Advanced composite materials and improved manufacturing processes are expected to not only enable the engine components to sustain higher pressure ratios and temperatures but also reduce the overall engine weight. This task investigates engine materials that increase the maximum temperature limit and provide weight savings. These material technologies include ceramic matrix composite (CMC) vanes, CMC exhaust core nozzle, polymer matrix composites (PMC), 1,500°F hybrid disk, 1,500°F non-contacting seal, advanced polymer matrix disk, lightweight CMC liner, advanced thermal barrier coatings, advanced turbine alloys, PMCs, and NASA GRX-810.

Advancements in Environmental Barrier Coatings (EBC) have enhanced the durability of CMCs, allowing lightweight CMC liners to function effectively in high-temperature, high-stress environments up to 3,159°R (NASA, n.d.). The CMC exhaust core nozzles can operate at temperatures up to 1,960 R for oxide/oxide CMC (Heim et al., 2013a). This allows the engine to extract more energy from combustion. CMC vanes provide higher temperature capability than conventional high-pressure turbine (HPT) vanes. They can withstand higher temperatures of up to 3,160 R without the need for extensive cooling (Heim et al., 2013b).

The hybrid disk is a 15 µm grain size low-solvus, high-refractory (LSHR) superalloy bore, and a new NASA low density single (LDS) crystal rim superalloy. The materials are tailored to meet the structural requirements of a disk with increased maximum operating temperature of 1,500°F for future high 50+ OPR engines, compared to the current 1,300°F maximum operating temperature (Hathaway et al., 2013).

The advanced polymer matrix disk made of single crystal superalloys offers improved mechanical properties and higher temperature capabilities. This disk increases maximum high-pressure compressor (HPC) exit temperature to 1,400°F. The single crystal nickel based-superalloy of the disk rim will be bonded to the powder metallurgy disk alloy with 1,400-1,450°F temperature capability creating an advanced hybrid disk system with up to 1,500°F temperature capability (Misra, 2012).

The advanced thermal barrier coatings (TBC), typically ceramic-based, support higher turbine inlet temperatures. They reduce the need for excessive cooling air by increasing the allowable metal temperature of the HPT component by 300°F (Padture & Gell, 2003). Advanced TBC systems have demonstrated increased T4 max up to 3,002°F, which is far beyond the current state-of-the-art baseline Yttria-stabilized zirconia ($ZrO_2$-$Y_2O_3$) thermal barrier and Barium Strontium Aluminum Silicate (BSAS)/mullite+BSAS environmental barrier coating capabilities (Zhu et al., 2008).

The advanced turbine alloys are nickel-based superalloys that operate at higher temperatures while maintaining mechanical integrity, allowing for increased turbine inlet temperatures (TIT). Specifically, these superalloys increase maximum HPT and low-pressure turbine (LPT) vane and blade temperatures by approximately 90°R from their baseline temperature (MacKay et al., 2009; Nathal, 2009).

Polymer matrix composites offer weight reductions, specifically to fan blades. PMCs made with PMR-15 resin have been incorporated in the blades of military engines since they have a continuous use temperature between 550°F to 600°F (McDanels et al., 1986; Wei et al., 2024). RP-46 high temperature polymide resin is NASA's advanced alternative, initially capable of withstanding 371°C (700°F+), but Navy SBIR independent testing showed that it could withstand temperatures up to 2,300°F (Langley Research Center, 2009).

The NASA **G**lenn **R**esearch Center e**X**treme temperature alloy (GRX-810) was developed using Integrated Computational Materials Engineering (ICME). GRX-810 is an oxide dispersion strengthened (ODS) alloy designed for sustained use at 900-1,200°C with high strength and 100 times stress rupture capabilities (Gradl et al., 2024). GRX-810 can endure higher temperatures and stress and can last up to 2,500 times longer compared to other nickel-based alloys. It also has about four times the tensile strength before breaking and twice as resistant to oxidation damage when exposed to oxygen-rich environments at high temperatures (Newbacher, 2024).

As part of the materials evolution literature review, historical thermal trends were analyzed to understand how turbine inlet temperature (T4) has progressed across generations of civil and military gas turbine engines. Publicly available temperature data were obtained from numerous sources to (1) inform the calibration process for engines included in this study and (2) improve prediction accuracy for future propulsion systems by constraining T4 to physically realistic values. Incorporating these dataset-driven temperature bounds reduces the degrees of freedom in the calibration process, thereby preventing nonphysical cycle solutions and enabling more accurate models. Figure 26, adapted from Heidmann (2011), illustrates the increasing T4 capability enabled by advancements in materials and cooling technologies over the last century, providing a valuable reference for establishing credible thermal limits during engine model development.

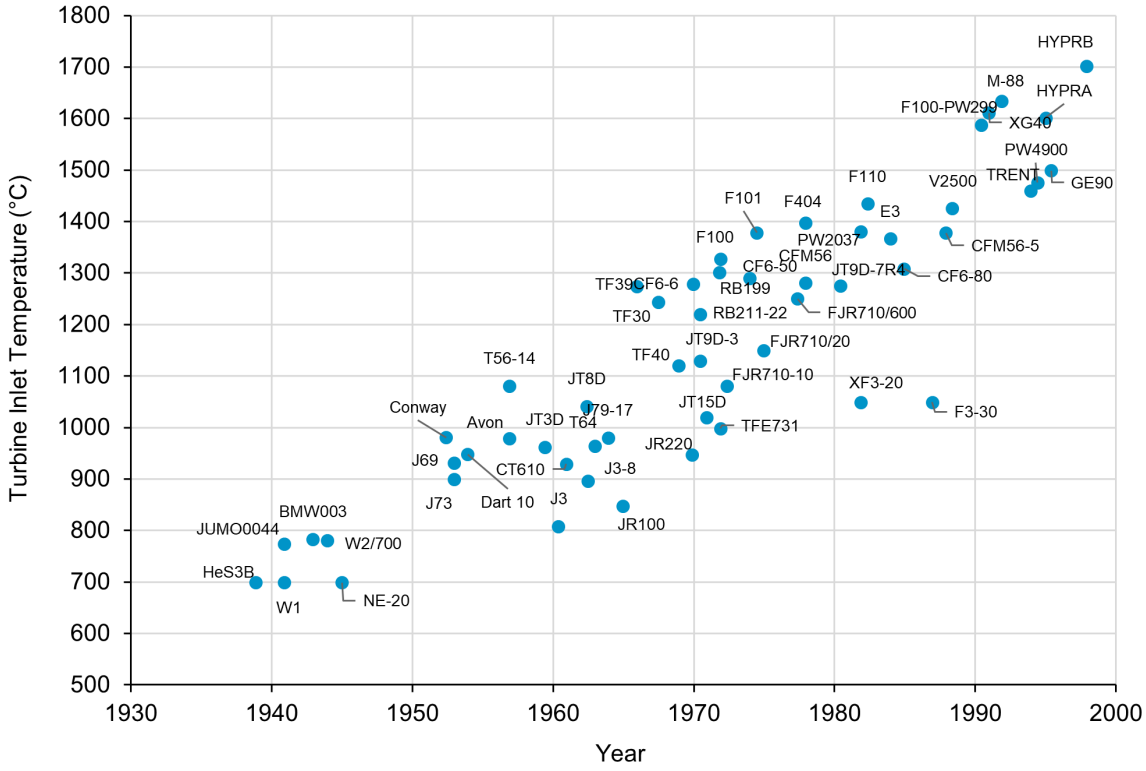


**Figure 26.** Engine thermal trends (turbine inlet temperature, T4).

To improve the accuracy of HPT blade temperature estimates, the evolution of material temperature capabilities was examined using data obtained from multiple published sources. The review covers historical and current turbine blade materials—including nickel-based superalloys, CMCs, titanium matrix composites, and PMCs as well as thermal and environmental coating systems. Figure 27, adapted from Misra et al. (2013), summarizes the progression of nickel-based superalloy temperature capability, highlighting the steady increase in allowable blade metal temperatures over time.

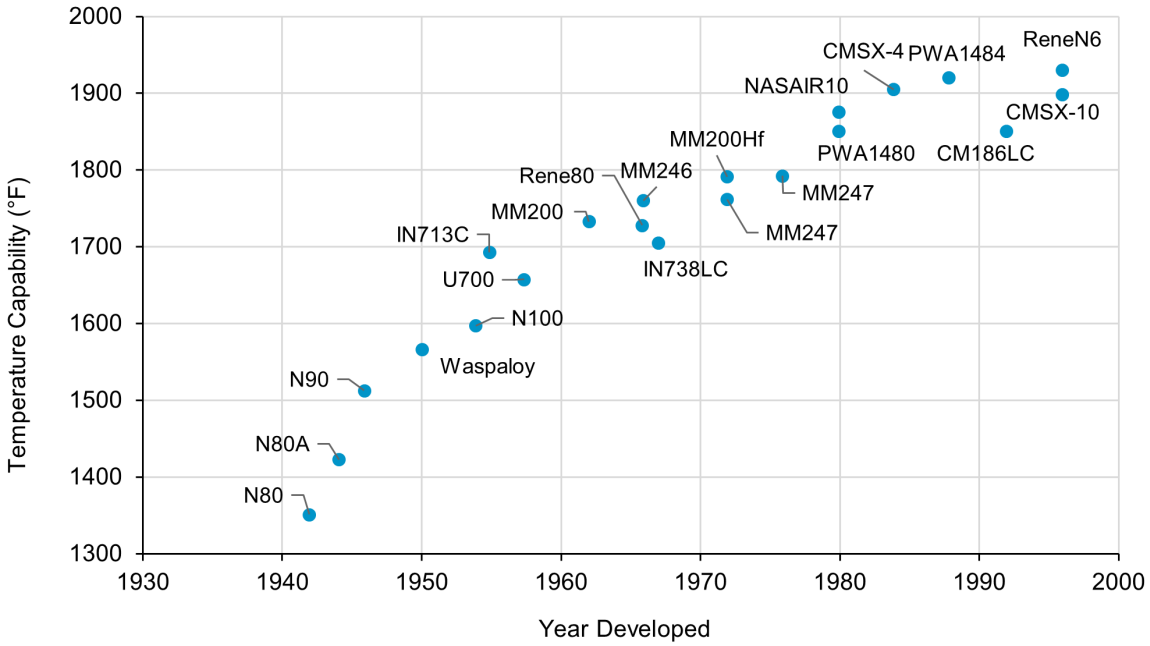


**Figure 27.** Temperature capabilities of nickel superalloys for turbine blade.

**Step 2 - Engine Efficiency Improvement**

With the advancement in engine design methods, engine materials, and engine manufacturing process, it is expected the thermal and propulsive efficiencies of gas turbine engines will be improved over the next few decades. To determine the possible performance boundary of the turbofan architecture, it is necessary to quantify the potential improvements in engine component efficiencies. The ICAO LTAG Report Appendix M3 Technology Subgroup Report (ICAO, 2022) provided a projection of efficiencies of engine core components in the years 2030, 2040, and 2050. The projection was made for different classes of aircraft, and for each class year, there are three levels of confidence: (1) conservative, (2) medium, and (3) aggressive. This task takes the 2050 aggressive prediction as the reference to maximize the improvements in core efficiencies to explore the boundary. Table 7 compares the efficiencies of engine components between the 2050 aggressive projection and the baseline Airbus A320neo model.

**Table 7.** Engine components' efficiencies. HPC: high-pressure compressor, HPT: high-pressure turbine, LPC: low-pressure compressor, LPT: low-pressure turbine).

| Component | Baseline Airbus A320neo Engine Model | LTAG 2050 Aggressive Prediction | Improvement |
|---|---|---|---|
| **Fan (adiabatic)** | 92.5% | 93.4% | +0.9% |
| **LPC (polytropic)** | 91.5% | 93.3% | +1.8% |
| **HPC (polytropic)** | 91.4% | 93.3% | +1.9% |
| **HPT (adiabatic)** | 89.0% | 90.7% | +1.7% |
| **LPT (adiabatic)** | 91.1% | 93.1% | +2.0% |

Propulsion technologies that contribute to advancement in engine design methods leading to improvement in engine component efficiencies include advanced compressors, advanced turbines, and active flow control integrated into the compressor and turbine. Advanced compressors and turbines are primarily designed to improve efficiency, performance, and durability using state-of-the-art materials, aerodynamics, and control mechanisms to achieve high-pressure ratios and

minimize energy losses. For the compressor, active flow control manages the boundary layer and reduces separation in both subsonic and supersonic conditions by adjusting the internal flow path. Pinto & G. (2024) demonstrated that active flow control techniques, such as tip injection, can improve the stall margin of compressors by 14.26% using a 0.3% total mass flow rate injection (Pinto & G, 2024). In a turbine, flow control increases loading and efficiency by injecting air around the turbine blades and near the end wall, in turn reducing the turbine stage count.

**Step 3 - Small Core Size Effect**

One contributing factor to the engine component efficiency is the core size effect. As the turbofan engine continues to strive for higher bypass ratios to promote propulsive efficiency, the core size is becoming smaller. Meanwhile, future airframe technologies will reduce the aircraft drag and the thrust required, encouraging smaller size engines for future aircraft. However, as the engine core becomes smaller, rotor tip clearance, knife-edge seal clearances, and edge thicknesses cannot be scaled down with the engine core size. All these non-scalable features introduce penalties to HPC efficiency. Figure 28, adopted from Evan et al. (2022), illustrates how HPC polytropic efficiency is affected by the engine core flow rate. The orange curve represents the current technology level, which is applied on the baseline A320neo model. The green curve is shifted from the orange curve by 25% improvement in HPC efficiency, as predicted by the LTAG study. This curve is utilized in the 2050 narrow-body aircraft engine model. The blue curve represents an ideal scenario where clearances can be scaled with the core size, which is used in a practical ideal engine model created in this task. All these curves are digitalized in EDS.

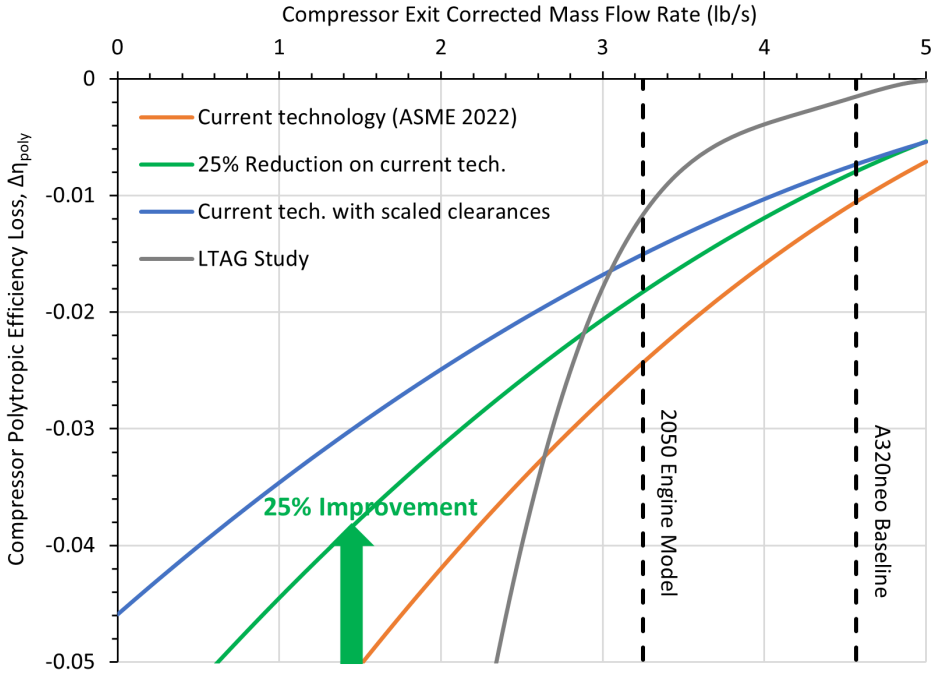


**Figure 28.** Engine core size effect on HPC.

Turbine size-effect losses were examined using publicly available studies on corrected mass-flow scaling and stage-level efficiency degradation. Data from Bettner's component arrangement studies and the more recent "Educated Guess" framework developed by the German Aerospace Center were obtained to characterize how HPT efficiency varies with turbine entry corrected mass flow rate. The Educated Guess study defines an efficiency envelope based on the Grieb coefficient ( $\lambda$ ), from which stage-specific curves are selected, while the Bettner (1990) studies provide historical and projected technology trends. All curves were normalized using a reference large-core flow rate of 10 lbm/s and incorporated into EDS to model turbine size-effect penalties within the design loop. Figure 29 presents these turbine size-effect loss curves and illustrates how reductions in turbine core flow introduce measurable efficiency penalties.

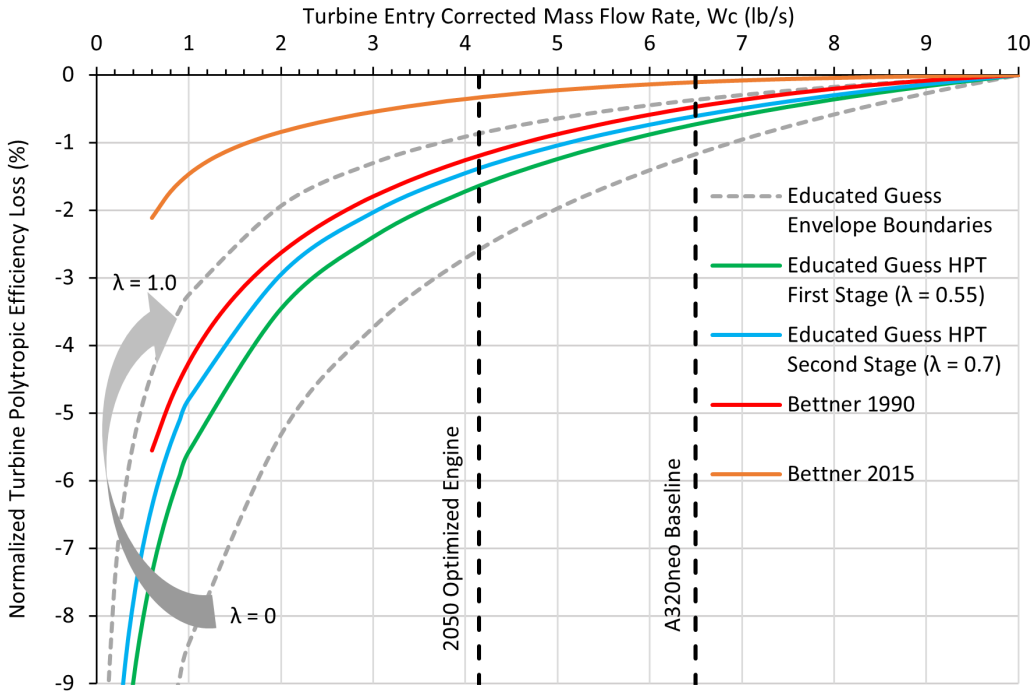


**Figure 29.** Engine core size effects on HPT.

Within the engine core, clearances can become significant during operation and allow more flow to bypass the blades. To meet the ICAO LTAG 2050 aggressive predictions for the compressor, implementing an active compressor clearance control mechanism can reduce clearance by adjusting the size of the casing. This would increase the compressor efficiency by reducing the amount of flow leakage up to 33% for a low-speed compressor cascade rig due to a Normal Synthetic Jet and Bae (2001). Active clearance control works by dynamically adjusting the position of the casing relative to the blade tip and maintains a certain clearance for each stage of the flight. For the turbine, an active clearance control would allow for dynamic tip clearance adjustments in response to thermal and mechanical deformations during engine operation. This would improve turbine efficiency by minimizing leakage losses while preventing blade-tip rubs. However, the efficiency improvements depend on actuator performance.

**Step 4 - Aircraft Systems Impacts**

Engine efficiency is also affected by the aircraft systems that consume pneumatic, hydraulic, electric, and mechanical power. These systems include but are not limited to environmental control system (ECS), ice protection system (IPS), aircraft control system, and avionic system. The pneumatic power is mainly provided by the bleed air extracted from the engine compressor. The hydraulic and electric power are mainly converted from the mechanical power extracted from the engine shaft. With the technological improvements in aircraft equipment systems and secondary power distribution systems, it is expected that less bleed air and power extractions will demand from the engine, improving the engine propulsive efficiency. The LTAG study predicted that the thrust-specific fuel consumption (TSFC) of the narrow-body aircraft engine at the aerodynamic design point would be reduced by 1.67% due to the improvements in bleed and power extraction, as listed in Table 8. Furthermore, enabled by the electrification of aircraft systems, bleed air from the engine compressor may not be needed. In the bleedless architecture, aircraft systems are mainly driven by the electric power converted from the mechanical power extracted from the engine shaft. Table 8 presents the engine TSFC improvement at different power extraction settings when the bleedless architecture is applied.

**Table 8.** Aircraft systems impact on engine TSFC.

| Architecture | Bleed | Power extraction | TSFC change |
|---|---|---|---|
| **Baseline A320neo** | 2 | 75 | -- |
| **2050 engine model** | 1.25 | 50 | -1.67% |
| **Bleedless architecture** | 0 | 250 | -2.57% |
| | 0 | 225 | -2.76% |
| | 0 | 200 | -2.96% |

**Step 5 - Engine Cycle Optimization**
The implementation of engine cooling technologies has a direct impact on an engine cycle by lowering compressor exit temperature (T3) and increasing turbine inlet temperature (T4). Compressor intercoolers increase T3 max constraint by 50-60 K before the compressed air enters the combustion chamber. Cooled cooling technology enables the handling of high heat fluxes, critical for engines, avionics, and other components in modern aircraft. With its implementation, the HPC bleed air is cooled by around 4.44%, so that the turbine inlet temperature, T4, increases from 1,860 K to 1,910 K (Zhang et al., 2022). Active film cooling allows for higher turbine inlet temperatures, which exceed 1,900 K/3,420°R in modern engines by decreasing the convective heat transfer to the turbine components such as guide vane, blades, turbine casing, and exhaust nozzle (Acharya & Kanani, 2017). As mentioned in Step 5, advanced engine materials also impact the engine cycle. The 1,500°F hybrid disk allows for a 50+ overall pressure ratio (OPR), and the advanced TBC systems have demonstrated an increased T4 max up to 3,462°R.

To maximize the benefits of these engine technologies, the engine needs to be resized with optimal cycle parameters. In this task, the engine cycle parameters include bypass ratio (BPR), OPR, fan pressure ratio (FPR), high-pressure compressor pressure ratio (HPCPR), and turbine entry temperature (T4max). The optimization process follows the steps described in Task 2, where surrogate models are developed based on the responses of the DoE sample cases run through the EDS. The objective function is to minimize the fuel burn of the notional Airbus A320neo model at an economic mission. Table 9 presents the optimized cycle of the 2050 engine and compares it to the baseline model.

**Table 9.** Optimized engine cycle parameters.

| Design Variable | Baseline Airbus A320neo Engine Model | Optimized 2050 Engine Cycle |
|---|---|---|
| **BPR** | 11.6 | 14.5 |
| **OPR** | 45.8 | 61.0 |
| **FPR** | 1.52 | 1.45 |
| **HPCPR** | 17.0 | 17.5 |
| **T4max (R)** | 3091 | 3144 |

**Step 6 - Fuel Burn Evaluation**
The possible boundary of the turbofan engine is evaluated based on the aircraft-level fuel consumption at an economical mission that is most frequently flown by the narrow-body aircraft. With Steps 2 to 6 implemented sequentially, several engine models are established and integrated with the notional A320neo aircraft model. The fuel burn is evaluated at the 900-nm mission with the design payload. The fuel reductions due to efficiency improvement, size effect reduction, aircraft system architecture, engine weight, and engine cycle optimization are evaluated in a stepwise manner.

## Milestones

- Finished literature review on turbofan engine efficiency, and the potential impacts of engine materials, engine cooling technologies, fan and inlet technologies, core size effects, and bleedless aircraft system architecture.
- Established 2050 narrow-body aircraft model based on the aggressive prediction made in the LTAG study.

- Created a practical ideal engine model by assuming scalable tip clearances, large-core efficiencies, and bleedless architecture on the 2050 engine model.

## Major Accomplishments

The major accomplishments of this task include the evaluations of contributions of different engine technologies to the fuel burn efficiency when retrofitting the state-of-the-art aircraft with a new turbofan engine, as well as the development of a practical ideal engine model to explore the boundary of the turbofan architecture.

Figure 30 displays the reductions of the 900-nm mission block fuel when engine technologies are progressively applied to the notional PW-1127G engine. Note that the airframe is maintained as the notional A320neo model during the evaluation, while only the engine model is updated. The practical ideal engine shown in the last bar is established by assuming bleedless architecture with 200 hp power extraction and scalable tip clearances on top of the aggressive core efficiency improvement prediction, engine weight reduction, and the application of advanced engine materials. Overall, with all potential engine technologies applied and the idealized core size effect, the turbofan engine can reduce the fuel burn at the economical mission by 20.7% for the A320neo aircraft compared to the current technology level. It is seen that the core efficiency improvement has made the most significant contribution to the engine fuel efficiency, reducing the economical mission block fuel by 7.7%. Meanwhile, engine cycle optimization also has a considerable impact on the fuel burn reduction due to the increased OPR and T4max and decreased FPR.

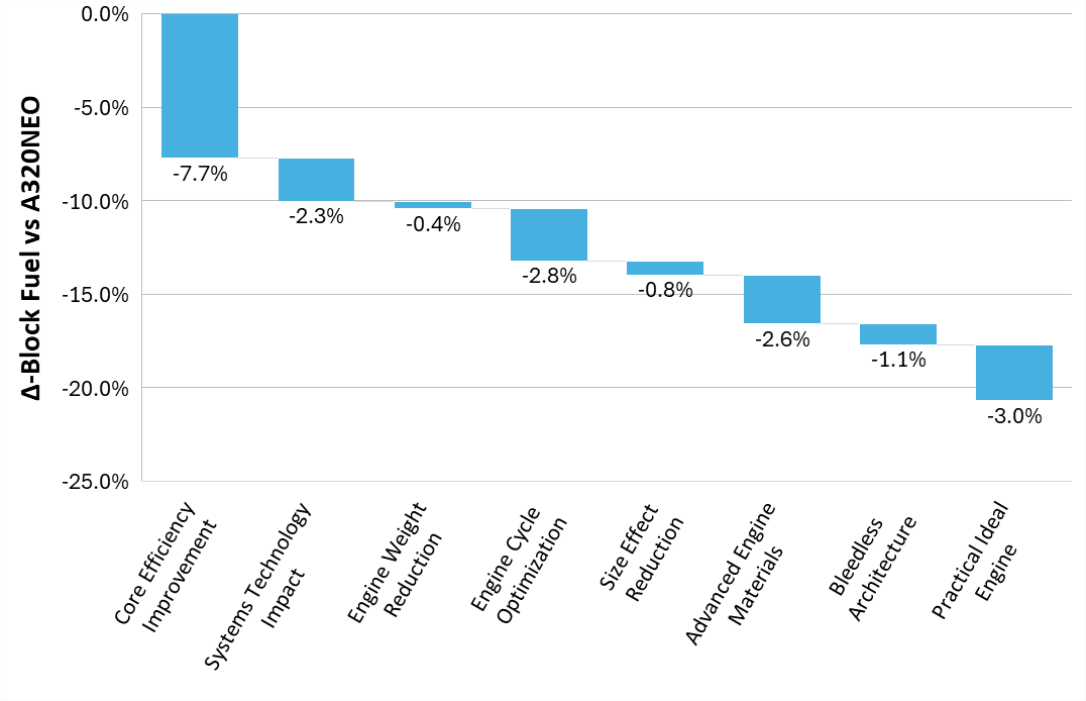


**Figure 30.** Potential block fuel reductions due to engine technologies.

## Publications

None.

## Outreach Efforts

- Attended ASCENT biannual meetings.

## Awards

None.

## Student Involvement

This task involves three graduate students: Cem Kocer, Emmanuella Okonkwo, and Akshiti Parashar

## Plans for Next Period

- Add inlet, fan, and nozzle technologies from the FAA's Continuous Lower Energy, Emissions and Noise (CLEEN) Program and other literatures to the 2050 "practical" ideal turbofan engine model.
- Investigate the impact of engine core size on HPT efficiency.
- Develop a parametric model to quantify secondary power extraction and subsystem weights within a bleedless architecture.
- Introduce logistic regression as a data-driven method for predicting engine component polytropic efficiencies to investigate the physics-based limitations of existing and retired turbofan engines.

## References


Acharya, S., Kanani, Y. (2017). Advances in Film Cooling Heat Transfer (Ch. 3, pp. 91–156). In *Advances in Heat Transfer*, (Vol. 49). Elsevier. https://doi.org/10.1016/bs.aiht.2017.10.001. Accessed 10 Mar. 2025.

Bettner, J. (1990, July). Component Arrangement Studies for an 8000 SHP Turboshaft High Technology Core. *26th Joint Propulsion Conference*, AIAA 1990-2398. https://doi.org/10.2514/6.1990-2398

Gradl, P. R., Tinker, D., Williams, B., Smith, T. M., & Kantzos, C. (2024, January). Extreme Temperature Additively Manufactured GRX-810 Alloy Development and Hot-fire Testing for Liquid Rocket Engines (AIAA-2024-0997). *2024 AIAA SciTech Forum*. https://doi.org/10.2514/6.2024-0997

Hathaway, M. D., Rosario, R. D., & Madavan, N. K. (2013). NASA Fixed Wing Project Propulsion Research and Technology Development Activities to Reduce Specific Energy Consumption. *49th AIAA/ASME/SAE/ASEE Joint Propulsion Conference*.

Heidmann, J. (2011*). Improving Engine Efficiency through Core Developments* [Conference presentation]. 49th AIAA Aerospace Sciences Meeting, American Institute of Aeronautics and Astronautics (AIAA), Orlando, Florida.

Heim, F. M., Halbig, M. C., & Salvatore, M. J. (2013a). *Evaluation of Ceramic Matrix Composite Technology for Aircraft Turbine Engine Applications* (NASA/TM-2013-10774). National Aeronautics and Space Administration, Glenn Research Center.

Heim, F. M., Halbig, M. C., & Salvatore, M. J. (2013b). *Ceramic Matrix Composite (CMC) Components for Aircraft Engines* (NASA/TM-2013-10774). National Aeronautics and Space Administration, Glenn Research Center.

ICAO. (2022). Report on the Feasibility of a Long-Term Aspirational Goal Appendix M3, Technology Subgroup Report. International Civil Aviation Organization.

Langley Research Center. (2009). *Polyimide/glass composite high-temperature insulation*. https://www.techbriefs.com/component/content/article/5002-lar-17321-1

MacKay, R., Gabb, T., Smialek, J., & Nathal, M. (2009). *Alloy Design Challenge: Development of Low Density Superalloys for Turbine Blade Applications* (NASA/TM-2009-215819). National Aeronautics and Space Administration.

McDanels, D. L., Serafini, T. T., & DiCarlo, J. A. (1986). Polymer, metal, and ceramic matrix composites for advanced aircraft engine applications. *Journal of materials for energy systems, 8*(1), 80-91.

Misra, A. K., & Greenbauer-Seng, L. A. (2013). Aerospace Propulsion and Power Materials and Structures Research at NASA Glenn Research Center. *Journal of Aerospace Engineering, 26*(2), 459–490. https://doi.org/10.1061/(ASCE)AS.1943-5525.0000325

Misra, K. (2012, October 15-18). *Durability Challenges for Next Generation of Gas Turbine Engine Materials* [Conference Paper]. AVT Symposium on Design, Modelling, Lifting and Validation of Advanced Materials in Extreme Military Environments, Biarritz, France.

NASA. (n.d.). *High-Temperature Environmental Barrier Coatings for SiC/SiC Ceramic Matrix Composites*. National Aeronautics and Space Administration, Technology Transfer Program, Patent LEW-TOPS-136. https://technology.nasa.gov/patent/lew-tops-136

Nathal, M. (2009). *High Temperature Turbine Materials*. 2009 Annual Meeting, Fundamental Aeronautics Program.

Newbacher, B. (2024). *NASA Licenses 3D-Printable Superalloy to Benefit US Economy*. National Aeronautics and Space Administration, Glenn Research Center.

Padture, N., & Gell, M. (2003). *Advanced Thermal Barrier Coatings for Industrial Gas Turbine Engines* (AGTSR Subcontract No. 00-01-SR081). Clemson University Research Foundation.

Pinto, P., & G, S. (2024). Performance Enhancement of an Axial Flow Compressor Using Active Flow Control Technique. *Cogent Engineering, 11*(1), 2380804. https://doi.org/10.1080/23311916.2024.2380804

Wei, Jiahui, Zhang, Y., Liu, Y., Wang, Y., Li, C., Sun, Z., Xu, H., Shao, H., Zhang, D., Zou, Q., Zhang, Q., Feng, J., Kong, W., Jiao, Y., & Chen, L. (2024). Advances in resin matrix composite fan blades for aircraft engines: a review. *Thin-Walled Structures, 202*, 112058. https://doi.org/10.1016/j.tws.2024.112058

Zhang, L., Xu, G., Liu, Q., Li, M., Dong, B., & Wen, J. (2022). Superiority Analysis of the Cooled Cooling Air Technology for Low-Grade Energy Utilization in Aircraft Engines. *Energy Conversion and Management, 252*, 115028.

Zhu, D., Miller, R., & Fox, D. (2008). *Thermal and Environmental Barrier Coating Development for Advanced Propulsion Engine Systems* (NASA/TM-2008-215040). National Aeronautics and Space Administration.